Telomere repeats induce domains of H3K27 methylation in Neurospora

Kirsty Jamieson[1,3], Kevin J. McNaught[1,3], Tereza Ormsby[1], Neena A. Leggett[1], Shinji Honda[2] and Eric U. Selker[1*]

[1]Institute of Molecular Biology, University of Oregon, Eugene, OR, USA 97403-1229

[2]Faculty of Medical Sciences, University of Fukui, Fukui, 910-1193 Japan

[3]These authors contributed equally to this work

[*]Corresponding author. Email: selker@uoregon.edu

Keywords: facultative heterochromatin/H3K27/telomere repeats/chromosome rearrangements/Polycomb/PRC2/telomerase/position effect

ABSTRACT

Development in higher organisms requires selective gene silencing, directed in part by di-/tri-methylation of lysine 27 on histone H3 (H3K27me2/3). Knowledge of the cues that control formation of such repressive Polycomb domains is extremely limited. We exploited natural and engineered chromosomal rearrangements in the fungus *Neurospora crassa* to elucidate the control of H3K27me2/3. Analyses of H3K27me2/3 in strains bearing chromosomal rearrangements revealed both position-dependent and position-independent facultative heterochromatin. We found that proximity to chromosome ends is necessary to maintain, and sufficient to induce, transcriptionally repressive, subtelomeric H3K27me2/3. We ascertained that such telomere-proximal facultative heterochromatin requires native telomere repeats and found that a short array of ectopic telomere repeats, $(TTAGGG)_{17,}$ can induce a large domain (~225 kb) of H3K27me2/3. This provides an example of a *cis*-acting sequence that directs H3K27 methylation. Our findings provide new insight into the relationship between genome organization and control of heterochromatin formation.

INTRODUCTION

Methylation of lysine 27 on histone H3 (H3K27me) has emerged as an important repressive mark of the Polycomb group (PcG) system, which is critical for development in higher organisms. PcG proteins were initially discovered in *Drosophila melanogaster* as repressors of homeotic (*HOX*) genes during early embryogenesis (Lewis 1978) and play integral roles in the maintenance of cellular identity and differentiation in a variety of eukaryotes. Moreover, dysfunction of the PcG system commonly leads to disease, including cancer (Piunti and Shilatifard 2016; Conway et al. 2015). Biochemical work demonstrated that PcG proteins form two distinct histone-modifying complexes known as Polycomb Repressive Complex 1 and 2 (PRC1 and PRC2) (Müller et al. 2002; Wang et al. 2004). PRC1 mono-ubiquitinates lysine 119 on histone H2A (H2AK119ub1) with its E3-ubiquitin ligase subunit, Ring1, while PRC2 catalyzes mono-, di-, and trimethylation of histone H3 lysine 27 (H3K27me1/2/3) by its SET-domain component, EZH2 (Müller et al. 2002; Wang et al. 2004). PRC2, but not PRC1, is widely conserved in eukaryotes, including the filamentous fungus *Neurospora crassa,* but is absent in some simple eukaryotes such as the well-studied yeasts *Saccharomyces cerevisiae* and *Schizosaccharomyces pombe* (Jamieson et al. 2013). H3K27me2/3 covers approximately 7% of the *N. crassa* genome, including about 1000 fully-covered genes, all of which are transcriptionally quiescent (Jamieson et al. 2013; Galazka et al. 2016). The greater than 200 H3K27me2/3 domains, which range from 0.5-107 kb, are widely distributed throughout the genome but are enriched at subtelomeric regions (Jamieson et al. 2013), as also reported for other fungi (Schotanus et al. 2015; Dumesic et al. 2015; Studt et al. 2016; Connolly et al. 2013).

In *D. melanogaster*, DNA regulatory regions known as Polycomb Response Elements (PREs) recruit PcG proteins to specific chromatin targets to maintain transcriptional silencing (Steffen and Ringrose 2014). In vertebrates and other organisms, however, the mechanism by which PcG proteins are directed to particular loci is elusive (Bauer et al. 2015). We show that the control of H3K27 methylation is fundamentally different from that of epigenetic marks in constitutive heterochromatin. Not only is the genomic distribution of H3K27 methylation much more plastic than that of H3K9 methylation (Jamieson et al. 2016; Mathieu et al. 2005; Deleris et al. 2012; Lindroth et al. 2008; Reddington et al. 2013; Hagarman et al. 2013; Wu et al. 2010),

but also, unlike DNA methylation and methylation of histone H3K9, which are faithfully methylated *de novo* when introduced at arbitrary ectopic genomic sites (Miao et al. 1994; Selker et al. 1987), we show that H3K27 methylation is often position-dependent. We further demonstrate that telomere repeats underpin the observed position effect on H3K27me by showing that loss of telomerase abolishes subtelomeric H3K27me2/3 and that artificial introduction of telomere repeats at an interstitial site triggers deposition of H3K27me2/3. That is, telomere repeats themselves are both necessary for subtelomeric H3K27me2/3 and sufficient to trigger ectopic H3K27 methylation at internal chromosomal sites.

RESULTS

Analyses of classical chromosome rearrangements suggest that proximity to a chromosome end is key to subtelomeric H3K27 methylation

To search for *cis*-acting sequences that trigger facultative heterochromatin formation in *N. crassa*, perhaps analogous to PREs in *D. melanogaster*, we dissected a 47 kb H3K27me2/3 domain on linkage group (LG) VIL. A series of eight, partially overlapping, three kb fragments from this domain were separately targeted to both the *his-3* and the *csr-1* euchromatic loci in a strain in which we had deleted the endogenous H3K27me2/3 domain (Figure S1A). H3K27me2/3 chromatin immunoprecipitation (ChIP) followed by qPCR demonstrated the absence of *de novo* H3K27me2/3 within all eight segments when transplanted to either *his-3* or *csr-1* (Figures S1B and C).

To address the possibility that the failure to induce H3K27me2/3 in the transplantation experiments was simply due to the size of the test fragments, we utilized strains with large chromosomal rearrangements (Perkins 1997). We first examined translocations that involved the H3K27me2/3 domain on LG VIL that we had dissected, starting with UK3-41, an insertional translocation strain that has an approximately 1.88 Mb segment of LG VR inserted into a distal position on LG VIL (Figure 1A). The translocation shifted most of LG VIL to a more interior chromosomal position. Interestingly, H3K27me2/3 ChIP-seq of UK3-41 showed an absence of H3K27me2/3 in the region that was displaced from the chromosome end (lost H3K27me2/3; indicated in orange in Figure 1A). This result is consistent with our finding that transplantation

of segments from this region did not induce methylation at *his-3* or *csr-1* and suggests that the normal methylation of this subtelomeric domain is position-dependent.

These results raised the question of whether H3K27me2/3 in this domain absolutely depends on its normal location, or whether the methylation would occur if the region were moved near another chromosome end. To address this possibility, we utilized OY350, a quasiterminal translocation that transfers a distal segment of LG VIL to the end of LG IR (Figure 1B). Analysis of OY350 by H3K27me2/3 ChIP-seq showed that the translocated LG VIL domain preserved its normal H3K27me2/3 distribution when placed adjacent to the adoptive telomere. This finding supported the hypothesis that H3K27me2/3 in this domain depends on its proximity to the chromosome end and suggested that this requirement is non-specific; the different chromosome end apparently substituted for the native one. A similar situation was observed on LG VIR in OY320 (Figure 1F).

The results described above suggested that proximity to a chromosome end may be sufficient to induce H3K27me. Interestingly, in addition to consistent losses of previously subtelomeric H3K27me2/3 in the examined genomic rearrangements, we identified new H3K27me2/3 domains at novel subtelomeric regions. Striking examples of *de novo* H3K27me2/3 were independently observed in seven genome rearrangements at their new chromosome ends (Figures 1B-E and S4A-C; marked in green). These novel domains of H3K27me2/3 extended an average of approximately 180 kb into the new subtelomeric regions. The only apparent exception concerns translocation UK2-32 (Figure S4A), which involved the left end of LG V with approximately one Mb of tandemly repeated rDNA that is not shown in the *N. crassa* genome assembly. Altogether, our survey of chromosomal translocations strongly suggests that chromosome ends promote the deposition of H3K27me on neighboring chromatin.

Identification of position-independent H3K27-methylated domains

While domains of H3K27me2/3 are enriched near the ends of chromosomes in *N. crassa*, substantial domains are also found elsewhere. To examine the possibility of position-independent H3K27me2/3 residing within LG VIR, we examined the distribution of H3K27me2/3

in two translocations that effectively moved LG VIR to the middle of a chromosome. ALS159 is a reciprocal translocation that shifted wild-type LG VIR approximately 4.5 Mb away from the new telomere (Figure 1C). Although the shifted segment lost the H3K27me2/3 that was previously closest to the chromosome end, the more internal H3K27me2/3 was unaffected by the translocation (Figure 1C). Similarly, when LG VIR was inserted in the middle of LG III in OY329 (Figure 1D), most of the H3K27me2/3 on LG VIR was retained. Again, the H3K27me2/3 that was originally closest to the telomere was lost, however, consistent with the idea that subtelomeric H3K27me2/3 domains depend on their proximity to the chromosome ends.

To determine if the retention of H3K27me2/3 from LG VIR was unique, we examined the position-dependence of two other H3K27me2/3 domains. In translocation NM149, approximately 600 kb of LG IIL was translocated onto the end of LG VR, effectively shifting the native right arm of LG V about 600 kb away from the chromosome end (Figure 1E). Like the behavior of LG VIR in ALS159 and OY329, losses of H3K27me2/3 occurred in the most distal section of LG VR, but most H3K27me2/3 was retained, even when moved away from the chromosome end. In addition, a large H3K27me2/3 domain on LG IIIR was shifted approximately 450 kb away from the chromosome end in OY320, yet it did not incur losses (Figure 1F). Taken together, these findings demonstrate that some H3K27me2/3 domains can be maintained when translocated to internal chromosomal sites, *i.e.* some H3K27me domains appear to be position-independent.

Cis-trans test on H3K27 methylation in a segmental duplication strain reveals position effect

The observation that some chromosomal segments that are normally marked with H3K27me2/3 lose the mark when translocated to another genomic location suggested that H3K27me2/3 can be position-dependent. It remained formally possible, however, that the loss of H3K27me2/3 was an indirect effect of the translocation, perhaps due to an altered transcriptional program. To examine the possibility that one or more *trans*-acting factors could be responsible for the loss of H3K27me2/3 in OY329, we crossed this strain, which is in an Oak Ridge (OR) background, to a highly polymorphic wild-type strain, Mauriceville (MV), to obtain progeny with a segmental duplication, *i.e.* with the OR translocated LG VIR domain inserted into

LG II in a strain that also contained the corresponding region on the native LG VI of MV (Figure 2A). The high density of single nucleotide polymorphisms (SNPs) in the MV background allowed us to separately map the H3K27me2/3 distribution in the translocated (OR) segment and the wild-type (MV) segment (Pomraning et al. 2011). SNP-parsed H3K27me2/3 ChIP-seq showed that the duplicated chromosomal segments have distinct H3K27me2/3 profiles (Figure 2B). The previously subtelomeric H3K27me2/3 that was lost in OY329 did not return in the duplication strain, nor was the loss in this region recapitulated on the native LG VIR of MV. The independent behavior of these homologous segments suggests that the loss of H3K27me2/3 in OY329 was not a result of *trans*-acting factors, but rather was a result of the translocation itself, *i.e.* it is a *bona fide* position effect.

Altered gene expression in regions with changed H3K27me2/3

Considering that H3K27me2/3 normally marks transcriptionally quiescent chromatin in *N. crassa* (Jamieson et al. 2013), it was of obvious interest to ascertain whether ectopic H3K27me2/3 resulting from chromosomal translocations could cause gene silencing. To determine if the loss or gain of H3K27me2/3 in the translocation strains activated or repressed gene expression, respectively, we performed poly-A mRNA sequencing on wild-type and seven translocation strains (ALS159, AR16, OY329, OY337, OY350, UK2-32, and UK3-41). Figures 3A and B show gene expression and associated H3K27me2/3 levels in the wild-type and translocation OY350 strains at representative regions where former subtelomeres were moved and new ones created. The gain of H3K27me2/3 on LG VIL in OY350, due to formation of a novel subtelomere, coincided with reduced transcript levels relative to wild-type (Figure 3A). Conversely, the loss of H3K27me2/3 on LG IR in OY350, due to shifting the subtelomeric region, was associated with an increase in transcript abundance compared to wild-type (Figure 3B). Results of qPCR analyses of select genes confirmed these findings (Figure S3). Indeed, a comprehensive analysis of poly-A mRNA-seq data from all seven translocation strains showed increases in gene expression at previously subtelomeric regions that lost H3K27me2/3 and decreases in gene expression at novel subtelomeres that gained H3K27me2/3 (Figure 3C).

These findings demonstrate that chromosomal rearrangements can cause marked changes in both H3K27me2/3 and gene expression of the affected regions.

Loss of telomerase abolishes subtelomeric H3K27me2/3

Our analyses of translocation strains demonstrated that domains of H3K27me2/3 can be position-dependent and suggested that a feature of chromosome ends directly or indirectly recruits H3K27me2/3 to subtelomeric regions. To investigate the basis of this, we utilized a mutant lacking the single telomerase reverse transcriptase (*tert*) that is responsible for all $(TTAGGG)_n$ telomere repeats normally found on all *N. crassa* chromosome ends (Wu et al. 2009). Southern analysis of the *tert* strain using a $(TTAGGG)_n$ probe revealed major reductions in the hybridization signals and showed that the majority of telomere fragments present in wild-type were either undetectable or greatly reduced in the mutant (Figure 4A). In *S. pombe*, the majority of *trt1*$^-$ (yeast homologue of *N. crassa tert*) survivors have circularized their chromosomes (Nakamura et al. 1998). To determine if *N. crassa tert* survivors also have circular chromosomes, we designed outwardly directed PCR primers to amplify sequences near the ends of each chromosome and tested whether fragments were generated by fusions of the right and left chromosome ends. Indeed, the *tert* genomic DNA, but not control DNA from a wild-type strain, supported amplification using the divergent primer pairs, confirming intra-chromosomal fusions (Figure 4B).

We performed H3K27me2/3 ChIP-seq to determine whether the subtelomeric domains of H3K27me2/3 were retained or lost in the *tert* strain and found clear evidence of loss of H3K27 methylation from chromosome ends (Figure 4C). With the exception of LG V, which is unique in that one of its ends is capped with approximately 150 copies of the approximately 9 kb rDNA repeat (Butler and Metzenberg 1990), all chromosomes lost their subtelomeric H3K27me2/3 domains, which typically extend tens of thousands of bp from their ends. Internal H3K27me2/3 domains were not noticeably altered (Figures 4C and S5). Sequencing *of tert* input DNA from the ChIP showed no reduction in coverage near the chromosome ends, confirming that the losses of H3K27me2/3 ChIP signal observed in *tert* are not caused by chromosome

degradation. We conclude that either $(TTAGGG)_n$ telomere repeats or linear chromosome ends are required for position-dependent domains of H3K27me2/3 in *N. crassa.*

Internal telomere repeats are sufficient to induce *de novo* H3K27me2/3

To determine if the presence of telomere repeats is sufficient to trigger the deposition of H3K27 methylation, telomere repeats, oriented in either direction, were targeted to the *csr-1* locus. Due to the repetitive nature of these sequences and our cloning strategy, strains containing a variable number of (TTAGGG) repeats could be obtained through homologous recombination. Sequencing of inserted DNA in eight independent transformants revealed that the number of inserted telomere repeats ranged from 5 to 17. Native *N. crassa* telomeres have an average of 20 repeats (Wu et al. 2009). H3K27me2/3 ChIP-qPCR demonstrated that ectopic telomere repeats are sufficient to induce local H3K27me2/3 (Figure 5A). Even insertion of $(TTAGGG)_8$ triggered some methylation and insertion of $(TTAGGG)_{17}$ led to a high level of H3K27me2/3. ChIP-seq on the $(TTAGGG)_{17}$ strain revealed new peaks as far as 170 kb from the insertion site and the semi-continuous H3K27me2/3 domain spanned approximately 225 kb including 30 genes (Figure 5B). This is comparable to the size of subtelomeric H3K27me2/3 domains that were lost in the *tert* strain.

DISCUSSION

The proper distribution of the facultative heterochromatin mark, H3K27me2/3, deposited by PRC2, is necessary for appropriate gene expression in a variety of plants, animals and fungi (Wiles and Selker 2016). Unfortunately, the control of H3K27 methylation remains largely unknown. In *D. melanogaster*, DNA elements known as PREs are important to define domains of H3K27me and associated silencing, but even in this organism, PREs are neither sufficient in all genomic contexts, nor fully penetrant (Cunningham et al. 2010; Horard et al. 2000). In addition, it was recently found that deletion of a well-studied PRE in *D. melanogaster* did not significantly affect either gene silencing or H3K27 methylation at its native locus (De et al. 2016). The control of H3K27 methylation is less defined in mammals, in which only a few

252 candidate PRE-like elements have been identified (Basu et al. 2014; Sing et al. 2009; Woo et al.
253 2010).

254 We took advantage of a relatively simple eukaryote bearing H3K27me, the filamentous
255 fungus *N. crassa*, to explore the control of this chromatin mark. Conveniently, H3K27me is non-
256 essential in this organism, in spite of being responsible for silencing scores of genes (Klocko et
257 al. 2016; Jamieson et al. 2013). Unlike the situation with constitutive heterochromatin in *N.*
258 *crassa* (Miao et al. 1994; Selker et al. 1987), we demonstrated that not all facultative
259 heterochromatin is entirely controlled by underlying sequence elements; transplanted gene-
260 sized segments of a H3K27me domain do not, in general, become faithfully H3K27-methylated.
261 However, translocations of large chromosomal segments revealed two distinct classes of
262 transcriptionally repressive H3K27me domains, position-dependent and position-independent.
263 Mechanistic insights from subsequent experiments defined these classes as telomere repeat-
264 dependent and telomere repeat-independent H3K27me. The identification of telomere repeats
265 as potent signals for H3K27 methylation represents a major advance in our understanding of
266 facultative heterochromatin formation in eukaryotes.

267 Our study took advantage of a collection of spontaneous and UV-induced chromosome
268 rearrangement strains of *N. crassa* that were primarily collected and characterized by David
269 Perkins (Perkins 1997). We surveyed representative rearrangement strains in which
270 chromosomal regions containing domains of H3K27me were translocated to novel genomic
271 positions. Strikingly, ChIP-seq revealed multiple cases in which subtelomeric H3K27me2/3
272 domains completely lost this modification when moved to an interior chromosomal location.
273 Indeed, no exceptions to this rule were found. Generation and analysis of a segmental
274 duplication strain containing differentially marked translocated and normal segments
275 confirmed that the changed distribution of H3K27me2/3 was a *bona fide* position effect rather
276 than an effect of a *trans*-acting factor (Figure 2). Moreover, new subtelomeric regions gained
277 H3K27me2/3 over sequences that were previously devoid of this mark (Figure 1). We conclude
278 that proximity to a chromosome end, *per se*, somehow induces deposition of H3K27me2/3 in
279 domains that can span hundreds of kilobases. Analyses of polyA+ mRNA from the strains
280 revealed losses of gene expression associated with the new H3K27me2/3 and gains in gene

281 expression in regions that lost this mark; *i.e.* the changes in H3K27me2/3 were reflected in
282 underlying gene expression levels (Figure 3).
283 Although gene silencing near chromosome ends, sometimes dubbed "telomere position
284 effect" (TPE) has been observed in fungi (Kyrion et al. 1993; Nimmo et al. 1994; Castaño et al.
285 2004; Smith et al. 2008; Shaaban et al. 2010), *D. melanogaster* (Doheny et al. 2008), *Mus*
286 *musculus* (Pedram et al. 2006), and human cells (Baur et al. 2001), previous studies did not
287 implicate H3K27me. Interestingly, the extent of heterochromatin spreading from telomeres in
288 *N. crassa* is substantially greater than previously reported. This could be due to the conspicuous
289 absence of canonical subtelomere sequences in *N. crassa* (Wu et al. 2009; Mefford and Trask
290 2002; Arnoult et al. 2012; Pryde and Louis 1999). Not all organisms that exhibit TPE have H3K27
291 methylation machinery, but in *D. melanogaster*, which does, systematic analysis of PcG mutants
292 demonstrated they do not disrupt telomere silencing (Doheny et al. 2008). In human cells, TPE
293 is thought to be mediated by histone deacetylation, H3K9 methylation, and heterochromatin
294 protein HP1α (Tennen et al. 2011; Arnoult et al. 2012). Although the phenomenon of TPE has
295 been studied for decades, our findings may reflect the first documented case of H3K27me-
296 mediated TPE.
297 The ability of chromosome ends to induce large domains of H3K27me2/3 in
298 chromosomal translocation strains motivated us to investigate the role of telomere sequences
299 in the establishment of facultative heterochromatin. We found that deletion of *tert*, the sole
300 telomerase reverse transcriptase gene, results in a dramatic loss of H3K27me2/3 at
301 subtelomeres, concomitant with loss of $(TTAGGG)_n$ repeats and chromosome circularization
302 (Figure 4). To directly test the possibility that telomere repeats can trigger domains of
303 H3K27me2/3, we inserted an array of telomere repeats at an interstitial site and used ChIP to
304 check induction of H3K27me2/3. We found that, indeed, even a 48 bp array, $(TTAGGG)_8$, could
305 induce some local H3K27me2/3. Remarkably, a 102 bp array, $(TTAGGG)_{17}$, induced an
306 H3K27me2/3 domain that covered approximately 225 kb, including 30 genes (Figure 5). These
307 results strongly suggest that wild-type subtelomeric H3K27me2/3 is dependent on telomere
308 repeats. The recruitment of PRC2 to telomere repeats may be a widespread phenomenon,
309 considering that enrichment of H3K27 methylation at telomeres has been observed in fungi

(Jamieson et al. 2013; Schotanus et al. 2015; Dumesic et al. 2015; Studt et al. 2016), plants (Baker et al. 2015; Vaquero-Sedas et al. 2012) and animals (Wirth et al. 2009). Indirect recruitment of PRC2 by telobox-binding transcription factors (Xiao et al. 2017) and direct binding of PRC2 to G-quadruplex RNA resulting from transcription of telomere repeats (Wang et al. 2017) represent possible molecular mechanisms.

In addition to telomere repeats capping the ends of chromosomes, telomere repeat-like elements are scattered interstitially in the genomes of many organisms (Ruiz-Herrera et al. 2008). In *N. crassa,* interstitial telomere sequences are rare, limited to less than four tandem repeats, and are not preferentially associated with H3K27me2/3 regions. While *S. cerevisiae* and *S. pombe* lack PRC2 components and H3K27me, their internal telomere repeat-like elements can promote heterochromatin formation (Zofall et al. 2016; Duan et al. 2016). The genome of *Nicotiana tabacum* also has heterochromatic internal telomere repeats, but they lack the H3K27 methylation present at genuine telomeres (Majerová et al. 2014). Curiously, insertion of about 130 telomere repeats in Chinese ovary cells failed to significantly alter local transcription (Kilburn et al. 2001). It should be interesting to study the effects of terminal and interstitial telomere repeats on heterochromatin formation in a variety of organisms.

We inferred the existence of position-independent H3K27 methylation from our observation that some H3K27me2/3 domains were unaffected when moved to ectopic chromosomal locations (*e.g.* see domains on LG IIIR in OY320, LG VR in NM149, and LG VIR in ALS159 and OY329; Figure 1). The recapitulation of normal H3K27me2/3 profiles at ectopic chromosomal sites is consistent with the possibility that these chromosomal regions contain *cis*-acting signals that trigger the deposition of H3K27 methylation, perhaps comparable to PREs in *D. melanogaster*. It will be of interest to define the presumptive elements responsible for such position-independent H3K27me. While there is no consensus sequence for PREs in *D. melanogaster*, they are composed of unique combinations of binding sites for a variety of factors (Judith A Kassis 2013). One DNA-binding factor known to affect PcG silencing in *D. melanogaster*, GRH, has an obvious homolog in *N. crassa* and could be a candidate for helping establish or maintain position-independent domains of H3K27me2/3 *via* sequence-specific interactions (Blastyák et al. 2006; Nevil et al. 2017; Paré et al. 2012). It remains possible that

deposition of H3K27 methylation at position-independent domains is not directed by sequence-specific elements. In this context, it is worth noting that inhibition of transcription, caused by either exposure to RNA polymerase II inhibitors (Riising et al. 2014) or deletion of a transcriptional start site (Hosogane et al. 2016) was found to promote the deposition of H3K27me in mammalian cells. Conceivably, the position-independent domains of H3K27me2/3 in *N. crassa* could be directed by blocs of inherently low-expressing genes or by some other feature of the region, such as its location in the nucleus, which may be controlled by yet undefined factors. The fact that only about 10% of H3K27me2/3-marked genes are upregulated when the sole H3K27 methyltransferase is removed supports the notion that transcriptional shut-off may precede PRC2 recruitment (Klocko et al. 2016; Jamieson et al. 2013). Still, low transcriptional activity cannot entirely explain the targeting of PRC2 in *N. crassa* since many low-expressed genes are not H3K27 methylated.

Genome rearrangements are a common occurrence in malignant cells and can drive tumorigenesis through the creation of gene fusions, enhancer hijacking and oncogene amplification (Hnisz et al. 2016). Our findings suggest that genome rearrangements associated with cancer may additionally impact gene expression through effects on facultative heterochromatin. Indeed, there are already some reports of human diseases being driven by position effects (Surace et al. 2014; Guilherme et al. 2016). A great deal of research has focused on how characteristics of local chromatin influence translocation breakpoint frequencies (Hogenbirk et al. 2016), but the effects of the resulting translocations on chromatin state are still ill-defined. Altogether, our work shows that changes in genome organization can have sweeping effects on both the distribution of an epigenetic mark and gene expression. Thus, chromosome rearrangements may have unappreciated roles in evolution and cancer etiology.

368

369

MATERIALS AND METHODS

Strains, media and growth conditions

N. crassa strains are listed in Table S1 and were grown and maintained according to standard procedures (Davis 2000). All genome rearrangement strains are available through the Fungal Genetics Stock Center (www.fgsc.net).

Deleting and targeting segments of LG VIL

A strain containing a 47.4 kb deletion of LG VIL (N4933) was constructed by homologous recombination using primers listed in Table S2 (Colot et al. 2006). For *his-3* constructs, segments from LG VIL were PCR-amplified from wild-type (N3752) genomic DNA with primers containing restriction enzyme sites (Table S2) and directly cloned into pCR (Life Technologies TA Cloning Kit), subcloned into the *his-3*-targeting vector pBM61 (Table S3) and transformed into *N. crassa* strain N5739 (Margolin et al. 1997). For *csr-1* replacements, segments from LG VIL were PCR-amplified from wild-type (N3752) genomic DNA with primers containing homology to the 5' and 3' flanks of the *csr-1* locus (Table S2). Amplified segments were subsequently assembled by PCR ("PCR-stitched") to the 5' and 3' flanks of the *csr-1* locus respectively. Stitched PCR products were co-transformed into *N. crassa* strain N2931 and transformants were selected on cyclosporin A-containing medium (Bardiya and Shiu 2007).

Knocking-out *tert*

The *nat1* gene with the *trpC* promoter was amplified by PCR using the pAL12-Lifeact as the template with primers 3902 and 1369. The 5' and 3' flanking fragments of the *tert* gene were amplified by PCR with primers 3406-3409, which have specific 29-bp overhang sequence with the 5' and 3' *nat1* gene with the *trpC* promoter. The three PCR products were gel-purified, combined and PCR-stitched with primers 3406 and 3409 to construct the knockout cassette. The cassette was gel-purified and transformed into a Δ*mus-51* strain (N2929) by electroporation and resulting strains were crossed with a *mus-51*$^{+}$ strain (N3752) to recover progeny with the wild-type allele of *mus-51*.

Targeting telomere repeats to *csr-1*

Concatamers of telomere repeats were amplified in a polymerase chain reaction lacking template as previously described (Wu et al. 2009). Resulting PCR products of ~500 bp were gel-purified and cloned into the pCR4-TOPO TA vector (Life Technologies TOPO TA Cloning kit for Sequencing). Telomere repeats from the cloning vector were PCR-stitched separately to 5' and 3' flanks of the *csr-1* locus. Stitched PCR products were co-transformed into strain N5739 and transformants were selected on cyclosporin A-containing medium (Bardiya and Shiu 2007).

ChIP and preparation of libraries

ChIP was performed as previously described (Jamieson et al. 2016). An anti-H3K27me2/3 antibody (Active Motif, 39535) was used for all experiments. ChIPs for Figures 1 and 3, and Figures S1-3 were performed in biological triplicate. Real-time qPCR was performed as previously described (Jamieson et al. 2013). ChIP-seq libraries were also prepared as previously described (Jamieson et al. 2016), except N51, N6089, N6228 and N6383 libraries were subjected to eight cycles of amplification. Sequencing was performed using the Illumina NextSeq 500 using paired-end 100 nucleotide reads for input chromatin and some ChIP experiments. The remainder of the ChIP experiments were sequenced using the Illumina HiSeq 2000 using single-end 100 nucleotide reads or the NextSeq500 using single-end 75 nucleotide reads. All sequences were mapped to the corrected *N. crassa* OR74A (NC12) genome (Galazka et al. 2016) using Bowtie2 (Langmead and Salzberg 2012). ChIP-seq read coverage was averaged over 100 bp sliding (50 bp increment) windows with BEDTools (Quinlan and Hall 2010) and normalized to wild-type by library size. ChIP-seq data were visualized with Gviz (Hahne and Ivanek 2016). Normalized H3K27me2/3 ChIP-seq data was displayed using a 350 or 500 bp sliding widow unless otherwise specified.

RNA isolation and preparation of libraries

RNA isolation and poly(A)-RNA enrichment, RNA-seq library preparation, and subsequent differential expression analysis were performed with replicate samples as previously described (Klocko et al. 2016). RNA-seq data were visualized with Gviz(Hahne and Ivanek 2016).

428

429 **Translocation breakpoint analyses**

430 Incongruous-paired and split-read alignments for input DNA samples were found using bwa-
431 mem. The discordant and split-read alignments were analyzed with LUMPY v0.2.9 to determine
432 the location of chromosomal breakpoints (Layer et al. 2014). A list of predicted breakpoints
433 with a minimum call weight of five was generated and calls with an evidence set score <0.05.
434 The chromosomal breakpoints were compared to mapping data determined by recombination
435 mapping (Perkins 1997), RFLP coverage and inverse PCR (http://hdl.handle.net/10603/68) to
436 remove calls that were not associated with the translocation of interest. PCR analyses of
437 genome rearrangements ALS159, NM149, OY329 and UK3-41 were consistent with predicted
438 breakpoint patterns.

439

440 **Southern analysis**

441 Southern hybridization analyses were performed as previously described (Miao et al. 2000).
442 *N. crassa* telomere restriction fragments were examined as described previously with a
443 HindIII/NotI double digest (Wu et al. 2009). Primers used to make probe are listed in Table S2.

444

445 **SNP Mapping**

446 ChIP-seq data for the duplication strain was converted into fasta format, trimmed to 70 nt, and
447 filtered for 70 nt long reads using FASTX-Toolkit (http://hannonlab.cshl.edu/fastx_toolkit).
448 Processed data was SNP-parsed with Hashmatch (Filichkin et al. 2010) using the Mauriceville-
449 Oakridge SNPome (fasta file listing both versions of each SNP) (Pomraning et al. 2011). The
450 SNPome file was modified to align with read lengths of 70 nt. Reads with perfect alignment to
451 either genome were kept and allocated into two files according to SNP mapping. Each file was
452 then converted back into fastq format using SeqTK 1.0 (https://github.com/lh3/seqtk) and
453 remapped with Bowtie2 to the genome corresponding with its SNP alignment. H3K27me2/3
454 profiles were displayed in IGV (Thorvaldsdottir et al. 2013) to examine the individual
455 H3K27me2/3 profiles for wild-type and rearranged chromosome segments.

456

Data availability

All ChIP-seq and RNA-seq data, as well as whole genome sequence data, will be available from the NCBI Gene Expression Omnibus (GEO) database (accessions:).

ACKNOWLEDGMENTS

We thank Heejeung Yoo for genotyping *csr-1* targeting strains. This study was supported by a National Institutes of Health grant (GM093061) to EUS and a grant to S.H. from the Japanese Program to Disseminate Tenure Tracking System, Ministry of Education, Culture, Sports, Science and Technology.

COMPETING INTERESTS

The authors declare no financial or non-financial competing interests.

REFERENCES

Arnoult N, Van Beneden A, Decottignies A. 2012. Telomere length regulates TERRA levels through increased trimethylation of telomeric H3K9 and HP1α. *Nature Structural & Molecular Biology* **19**: 948–956.

Baker K, Dhillon T, Colas I, Cook N, Milne I, Milne L, Bayer M, Flavell AJ. 2015. Chromatin state analysis of the barley epigenome reveals a higher-order structure defined by H3K27me1 and H3K27me3 abundance. *Plant J* **84**: 111–124.

Bardiya N, Shiu PKT. 2007. Cyclosporin A-resistance based gene placement system for *Neurospora crassa*. *Fungal Genet Biol* **44**: 307–314.

Basu A, Dasari V, Mishra RK, Khosla S. 2014. The CpG island encompassing the promoter and first exon of human DNMT3L gene is a PcG/TrX response element (PRE). ed. R. Feil. *PLoS ONE* **9**: e93561.

Bauer M, Trupke J, Ringrose L. 2015. The quest for mammalian Polycomb response elements: are we there yet? *Chromosoma* **125**: 1–26.

Baur JA, Zou Y, Shay JW, Wright WE. 2001. Telomere position effect in human cells. *Science* **292**: 2075–2077.

Blastyák A, Mishra RK, Karch F, Gyurkovics H. 2006. Efficient and specific targeting of Polycomb group proteins requires cooperative interaction between Grainyhead and Pleiohomeotic. *Molecular and cellular biology* **26**: 1434–1444.

Butler DK, Metzenberg RL. 1990. Expansion and contraction of the nucleolus organizer region of Neurospora: changes originate in both proximal and distal segments. *Genetics* **126**: 325–333.

Castaño I, Pan S-J, Zupancic M, Hennequin C, Dujon B, Cormack BP. 2004. Telomere length control and transcriptional regulation of subtelomeric adhesins in *Candida glabrata*. *Mol Microbiol* **55**: 1246–1258.

Colot HV, Park G, Turner GE, Ringelberg C, Crew CM, Litvinkova L, Weiss RL, Borkovich KA, Dunlap JC. 2006. A high-throughput gene knockout procedure for *Neurospora* reveals functions for multiple transcription factors. *PNAS* **103**: 10352–10357.

Connolly LR, Smith KM, Freitag M. 2013. The *Fusarium graminearum* histone H3 K27 methyltransferase KMT6 regulates development and expression of secondary metabolite gene clusters. ed. H.D. Madhani. *PLOS Genet* **9**: e1003916.

Conway E, Healy E, Bracken AP. 2015. PRC2 mediated H3K27 methylations in cellular identity and cancer. *Curr Opin Cell Biol* **37**: 42–48.

503 Cunningham MD, Brown JL, Kassis JA. 2010. Characterization of the Polycomb Group Response
504 Elements of the *Drosophila melanogaster* invected Locus. *Molecular and cellular biology* **30**:
505 820–828.

506 Davis RH. 2000. *Neurospora: contributions of a model organism*. Oxford University Press.

507 De S, Mitra A, Cheng Y, Pfeifer K, Kassis JA. 2016. Formation of a Polycomb-domain in the
508 absence of strong Polycomb response elements. *PLOS Genet* **12**: e1006200.

509 Deleris A, Stroud H, Bernatavichute Y, Johnson E, Klein G, Schubert D, Jacobsen SE. 2012. Loss of
510 the DNA methyltransferase MET1 Induces H3K9 hypermethylation at PcG target genes and
511 redistribution of H3K27 trimethylation to transposons in Arabidopsis thaliana. ed. A.C.
512 Ferguson-Smith. *PLOS Genet* **8**: e1003062.

513 Doheny JG, Mottus R, Grigliatti TA. 2008. Telomeric position effect--a third silencing mechanism
514 in eukaryotes. *PLoS ONE* **3**: e3864.

515 Duan Y-M, Zhou BO, Peng J, Tong X-J, Zhang Q-D, Zhou J-Q. 2016. Molecular dynamics of de
516 novo telomere heterochromatin formation in budding yeast. *J Genet Genomics* **43**: 451–
517 465.

518 Dumesic PA, Homer CM, Moresco JJ, Pack LR, Shanle EK, Coyle SM, Strahl BD, Fujimori DG,
519 Yates JR III, Madhani HD. 2015. Product Binding Enforces the Genomic Specificity of a Yeast
520 Polycomb Repressive Complex. *Cell* **160**: 204–218.

521 Filichkin SA, Priest HD, Givan SA, Shen R, Bryant DW, Fox SE, Wong WK, Mockler TC. 2010.
522 Genome-wide mapping of alternative splicing in *Arabidopsis thaliana*. *Genome Res* **20**: 45–
523 58.

524 Galazka JM, Klocko AD, Uesaka M, Honda S, Selker EU, Freitag M. 2016. *Neurospora*
525 chromosomes are organized by blocks of importin alpha-dependent heterochromatin that
526 are largely independent of H3K9me3. *Genome Res* **26**: 1069–1080.

527 Guilherme RS, Moysés-Oliveira M, Dantas AG, Meloni VA, Colovati ME, Kulikowski LD,
528 Melaragno MI. 2016. Position effect modifying gene expression in a patient with ring
529 chromosome 14. *J Appl Genet* **57**: 183–187.

530 Hagarman JA, Motley MP, Kristjansdottir K, Soloway PD. 2013. Coordinate regulation of DNA
531 methylation and H3K27me3 in mouse embryonic stem cells. ed. J.G. Knott. *PLoS ONE* **8**:
532 e53880.

533 Hahne F, Ivanek R. 2016. Visualizing genomic data using Gviz and Bioconductor. *Methods Mol*
534 *Biol* **1418**: 335–351.

535 Hnisz D, Weintraub AS, Day DS, Valton A-L, Bak RO, Li CH, Goldmann J, Lajoie BR, Fan ZP, Sigova
536 AA, et al. 2016. Activation of proto-oncogenes by disruption of chromosome

neighborhoods. *Science* **351**: 1454–1458.

Hogenbirk MA, Heideman MR, de Rink I, Velds A, Kerkhoven RM, Wessels LFA, Jacobs H. 2016. Defining chromosomal translocation risks in cancer. *Proc Natl Acad Sci USA* **113**: E3649–56.

Horard B, Tatout C, Poux S. 2000. Structure of a polycomb response element and in vitro binding of polycomb group complexes containing GAGA factor. *Molecular and cellular …*.

Hosogane M, Funayama R, Shirota M, Nakayama K. 2016. Lack of Transcription Triggers H3K27me3 Accumulation in the Gene Body. *Cell Rep* **16**: 696–706.

Jamieson K, Rountree MR, Lewis ZA, Stajich JE, Selker EU. 2013. Regional control of histone H3 lysine 27 methylation in Neurospora. *Proc Natl Acad Sci USA* **110**: 6027–6032.

Jamieson K, Wiles ET, McNaught KJ, Sidoli S, Leggett N, Shao Y, Garcia BA, Selker EU. 2016. Loss of HP1 causes depletion of H3K27me3 from facultative heterochromatin and gain of H3K27me2 at constitutive heterochromatin. *Genome Res* **26**: 97–107.

Judith A Kassis JLB. 2013. Polycomb Group Response Elements in *Drosophila* and Vertebrates. *Advances in genetics* **81**: 83–118.

Kilburn AE, Shea MJ, Sargent RG, Wilson JH. 2001. Insertion of a telomere repeat sequence into a mammalian gene causes chromosome instability. *Molecular and cellular biology* **21**: 126–135.

Klocko AD, Ormsby T, Galazka JM, Leggett NA, Uesaka M, Honda S, Freitag M, Selker EU. 2016. Normal chromosome conformation depends on subtelomeric facultative heterochromatin in *Neurospora crassa*. *Proc Natl Acad Sci USA* **113**: 15048–15053.

Kyrion G, Liu K, Liu C, Lustig AJ. 1993. RAP1 and telomere structure regulate telomere position effects in *Saccharomyces cerevisiae*. *Genes & development* **7**: 1146–1159.

Langmead B, Salzberg SL. 2012. Fast gapped-read alignment with Bowtie 2. *Nat Methods* **9**: 357–359.

Layer RM, Chiang C, Quinlan AR, Hall IM. 2014. LUMPY: a probabilistic framework for structural variant discovery. *Genome Biol* **15**: 1–19.

Lewis EB. 1978. A gene complex controlling segmentation in Drosophila. *Nature* **276**: 565–570.

Lindroth AM, Park YJ, McLean CM, Dokshin GA, Persson JM, Herman H, Pasini D, Miró X, Donohoe ME, Lee JT, et al. 2008. Antagonism between DNA and H3K27 methylation at the imprinted Rasgrf1 locus. ed. B. Van Steensel. *PLOS Genet* **4**: e1000145.

Majerová E, Mandáková T, Vu GTH, Fajkus J, Lysak MA, Fojtová M. 2014. Chromatin features of plant telomeric sequences at terminal vs. internal positions. *Front Plant Sci* **5**: 593.

569 Margolin BS, Freitag M, Selker EU. 1997. Improved plasmids for gene targeting at the *his-3* locus
570 of *Neurospora crassa* by electroporation. *Fungal Genetics Reports* 34–36.

571 Mathieu O, Probst AV, Paszkowski J. 2005. Distinct regulation of histone H3 methylation at
572 lysines 27 and 9 by CpG methylation in *Arabidopsis*. *The EMBO Journal* **24**: 2783–2791.

573 Mefford HC, Trask BJ. 2002. The complex structure and dynamic evolution of human
574 subtelomeres. *Nature Reviews Genetics* **3**: 91–102.

575 Miao VP, Singer MJ, Rountree MR, Selker EU. 1994. A targeted-replacement system for
576 identification of signals for *de novo* methylation in *Neurospora crassa*. *Molecular and*
577 *cellular biology* **14**: 7059–7067.

578 Miao VPW, Freitag M, Selker EU. 2000. Short TpA-rich segments of the ζ-η region induce DNA
579 methylation in *Neurospora crassa*. *Journal of molecular biology* **300**: 249–273.

580 Müller J, Hart CM, Francis NJ, Vargas ML, Sengupta A, Wild B, Miller EL, O'Connor MB, Kingston
581 RE, Simon JA. 2002. Histone methyltransferase activity of a *Drosophila* Polycomb group
582 repressor complex. *Cell* **111**: 197–208.

583 Nakamura TM, Cooper JP, Cech TR. 1998. Two modes of survival of fission yeast without
584 telomerase. *Science*.

585 Nevil M, Bondra ER, Schulz KN, Kaplan T, Harrison MM. 2017. Stable binding of the conserved
586 transcription factor grainy head to its target genes throughout *Drosophila melanogaster*
587 development. *Genetics* **205**: 605–620.

588 Nimmo ER, Cranston G, Allshire RC. 1994. Telomere-associated chromosome breakage in fission
589 yeast results in variegated expression of adjacent genes. *The EMBO Journal* **13**: 3801–3811.

590 Paré A, Kim M, Juarez MT, Brody S, McGinnis W. 2012. The functions of grainy head-like
591 proteins in animals and fungi and the evolution of apical extracellular barriers. *PLoS ONE* **7**:
592 e36254.

593 Pedram M, Sprung CN, Gao Q, Lo AWI, Reynolds GE, Murnane JP. 2006. Telomere position
594 effect and silencing of transgenes near telomeres in the mouse. *Molecular and cellular*
595 *biology* **26**: 1865–1878.

596 Perkins DD. 1997. Chromosome rearrangements in *Neurospora* and other filamentous fungi.
597 *Adv Genet* **36**: 239–398.

598 Piunti A, Shilatifard A. 2016. Epigenetic balance of gene expression by Polycomb and COMPASS
599 families. *Science* **352**: aad9780 1–15.

600 Pomraning KR, Smith KM, Freitag M. 2011. Bulk segregant analysis followed by high-throughput
601 sequencing reveals the *Neurospora* cell cycle gene, *ndc-1*, to be allelic with the gene for

ornithine decarboxylase, *spe-1*. *Eukaryotic Cell* **10**: 724–733.

Pryde FE, Louis EJ. 1999. Limitations of silencing at native yeast telomeres. *The EMBO Journal* **18**: 2538–2550.

Quinlan AR, Hall IM. 2010. BEDTools: a flexible suite of utilities for comparing genomic features. *Bioinformatics* **26**: 841–842.

Reddington JP, Perricone SM, Nestor CE, Reichmann J, Youngson NA, Suzuki M, Reinhardt D, Dunican DS, Prendergast JG, Mjoseng H, et al. 2013. Redistribution of H3K27me3 upon DNA hypomethylation results in de-repression of Polycomb target genes. *Genome Biol* **14**: R25.

Riising EM, Comet I, Leblanc B, Wu X, Johansen JV, Helin K. 2014. Gene silencing triggers polycomb repressive complex 2 recruitment to CpG islands genome wide. *Molecular cell* **55**: 347–360.

Ruiz-Herrera A, Nergadze SG, Santagostino M, Giulotto E. 2008. Telomeric repeats far from the ends: mechanisms of origin and role in evolution. *Cytogenetic and Genome Research* **122**: 219–228.

Schotanus K, Soyer JL, Connolly LR, Grandaubert J, Happel P, Smith KM, Freitag M, Stukenbrock EH. 2015. Histone modifications rather than the novel regional centromeres of *Zymoseptoria tritici* distinguish core and accessory chromosomes. *Epigenetics & Chromatin* **8**: 1.

Selker EU, Jensen BC, Richardson GA. 1987. A portable signal causing faithful DNA methylation *de novo* in *Neurospora crassa*. *Science* **238**: 48–53.

Shaaban M, Palmer JM, El-Naggar WA, El-Sokkary MA, Habib E-SE, Keller NP. 2010. Involvement of transposon-like elements in penicillin gene cluster regulation. *Fungal Genetics and Biology* **47**: 423–432.

Sing A, Pannell D, Karaiskakis A, Sturgeon K, Djabali M, Ellis J, Lipshitz HD, Cordes SP. 2009. A vertebrate Polycomb response element governs segmentation of the posterior hindbrain. *Cell* **138**: 885–897.

Smith KM, Kothe GO, Matsen CB, Khlafallah TK, Adhvaryu KK, Hemphill M, Freitag M, Motamedi MR, Selker EU. 2008. The fungus *Neurospora crassa* displays telomeric silencing mediated by multiple sirtuins and by methylation of histone H3 lysine 9. *Epigenetics & Chromatin* **1**: 5.

Steffen PA, Ringrose L. 2014. What are memories made of? How Polycomb and Trithorax proteins mediate epigenetic memory. *Nat Rev Mol Cell Biol* **15**: 340–356.

Studt L, Rösler SM, Burkhardt I, Arndt B, Freitag M, Humpf H-U, Dickschat JS, Tudzynski B. 2016. Knock-down of the methyltransferase Kmt6 relieves H3K27me3 and results in induction of cryptic and otherwise silent secondary metabolite gene clusters in *Fusarium fujikuroi*.

636 *Environ Microbiol* **18**: 4037–4054.

637 Surace C, Berardinelli F, Masotti A, Roberti MC, Da Sacco L, D'Elia G, Sirleto P, Digilio MC,
638 Cusmai R, Grotta S, et al. 2014. Telomere shortening and telomere position effect in mild
639 ring 17 syndrome. *Epigenetics & Chromatin* **7**: 1.

640 Tennen RI, Bua DJ, Wright WE, Chua KF. 2011. SIRT6 is required for maintenance of telomere
641 position effect in human cells. *Nat Commun* **2**: 433.

642 Thorvaldsdottir H, Robinson JT, Mesirov JP. 2013. Integrative Genomics Viewer (IGV): high-
643 performance genomics data visualization and exploration. *Brief Bioinformatics* **14**: 178–192.

644 Vaquero-Sedas MI, Luo C, Vega-Palas MA. 2012. Analysis of the epigenetic status of telomeres
645 by using ChIP-seq data. *Nucleic Acids Res* **40**: e163–e163.

646 Wang H, Wang L, Erdjument-Bromage H, Vidal M, Tempst P, Jones RS, Zhang Y. 2004. Role of
647 histone H2A ubiquitination in Polycomb silencing. *Nature* **431**: 873–878.

648 Wang X, Goodrich KJ, Gooding AR, Naeem H, Archer S, Paucek RD, Youmans DT, Cech TR,
649 Davidovich C. 2017. Targeting of Polycomb Repressive Complex 2 to RNA by short repeats
650 of consecutive guanines. *Molecular cell* **65**: 1056–1067.

651 Wiles ET, Selker EU. 2016. H3K27 methylation: a promiscuous repressive chromatin mark. *Curr*
652 *Opin Genet Dev* **43**: 31–37.

653 Wirth M, Paap F, Fischle W, Wenzel D, Agafonov DE, Samatov TR, Wisniewski JR, Jedrusik-Bode
654 M. 2009. HIS-24 linker histone and SIR-2.1 deacetylase induce H3K27me3 in the
655 *Caenorhabditis elegans* germ line. *Molecular and cellular biology* **29**: 3700–3709.

656 Woo CJ, Kharchenko PV, Daheron L, Park PJ, Kingston RE. 2010. A region of the human HOXD
657 cluster that confers polycomb-group responsiveness. *Cell* **140**: 99–110.

658 Wu C, Kim Y-S, Smith KM, Li W, Hood HM, Staben C, Selker EU, Sachs MS, Farman ML. 2009.
659 Characterization of chromosome ends in the filamentous fungus *Neurospora crassa*.
660 *Genetics* **181**: 1129–1145.

661 Wu H, Coskun V, Tao J, Xie W, Ge W, Yoshikawa K, Li E, Zhang Y, Sun YE. 2010. Dnmt3a-
662 dependent nonpromoter DNA methylation facilitates transcription of neurogenic genes.
663 *Science* **329**: 444–448.

664 Xiao J, Jin R, Yu X, Shen M, Wagner JD, Pai A, Song C, Zhuang M, Klasfeld S, He C, et al. 2017. Cis
665 and trans determinants of epigenetic silencing by Polycomb repressive complex 2 in
666 Arabidopsis. *Nature Genetics* **81**: 83.

667 Zofall M, Smith DR, Mizuguchi T, Dhakshnamoorthy J, Grewal SIS. 2016. Taz1-Shelterin
668 promotes facultative heterochromatin assembly at chromosome-internal sites containing

late replication origins. *Molecular cell* **62**: 862–874.

FIGURE LEGENDS

Figure 1. Chromosomal rearrangements are associated with altered H3K27me2/3. (A-F) Schematics show the movement (magenta curved arrows) of translocated segments and the resulting chromosomal rearrangements for six translocation strains. ChIPs were done on biological triplicates and pooled for sequencing. Blue and dashed lines distinguish source of chromosome while arrowheads indicate directionality of rearranged segments. H3K27me2/3 ChIP-seq tracks of WT and translocation strains are displayed above chromosome diagrams with zoom-in sections in boxes. H3K27me2/3 signals that were lost in translocation strains are shown in orange, H3K27me2/3 signals gained are indicated in green and invariant H3K27me2/3 signals are shown in black. Circles indicate centromeres. Gains and losses of H3K27me2/3 were confirmed by qPCR (Figure S2).

Figure 2. A segmental duplication confirms H3K27me2/3 position effect. (A) Diagram of a cross between the OY329 (Oak Ridge) insertional translocation strain and a polymorphic wild-type strain (Mauriceville), resulting in a strain bearing a duplicated chromosomal segment (outlined by rectangles). H3K27me2/3 ChIP-seq tracks (single experiment) and chromosomes are shown in black for the Oak Ridge strain and blue for Mauriceville. Solid and dashed lines indicate chromosome source. (B) Expanded view of the duplicated chromosome segment in parental strains and duplication-containing offspring along with associated SNP-parsed H3K27me2/3 profiles.

Figure 3. Altered gene expression reflects changes in H3K27me2/3. (A) Reduced gene expression in novel subtelomeric region (LG VIL) that gains H3K27me2/3 in translocation OY350. The top panel displays H3K27me2/3 ChIP-seq reads of OY350 (green) normalized to the corresponding the non-translocated segment in WT (black). The bottom panel shows

698 normalized mRNA-seq read counts (counts/1000) for genes (gray arrows) in the region for WT
699 (black) and OY350 (green). ChIP-seq data are from pooled biological triplicates; RNA-seq data
700 are from biological duplicates (B) Shifting a normally subtelomeric region to an internal position
701 in translocation OY350 results in loss of H3K27me2/3 on LG IR and increased gene expression.
702 The top panel displays H3K27me2/3 ChIP-seq reads of OY350 (orange) normalized to WT
703 (black). The bottom panel shows normalized mRNA-seq read counts (counts/1000) for genes
704 (gray arrows) in the region for WT (black) and OY350 (orange). (C) A box plot summarizes the
705 relationship between gain (green) or loss (orange) of H3K27me2/3 in seven chromosomal
706 translocation strains (ALS159, AR16, OY329, OY337, OY350, UK2-32, and UK3-41) and
707 associated gene expression changes ($\log_2$[translocation/WT]) within the corresponding
708 domains. The control (gray) represents gene expression in regions that do not exhibit changes
709 in H3K27me2/3.
710
711 **Figure 4. Loss of *tert* disrupts chromosome ends and abolishes subtelomeric H3K27me2/3**. (A)
712 Southern hybridization of genomic DNA from WT and *tert* strains digested with *Hind*III/*Not*I
713 reveals loss of chromosome ends marked with the telomere repeats $(TTAGGG)_n$, which was
714 used as the probe. The ethidium bromide (EtBr) image demonstrates equal loading of WT and
715 *tert* genomic DNA. (B) Circularization of chromosomes was demonstrated by generation of PCR
716 products with outwardly directed primers near chromosome ends in a *tert* strain, but not a WT
717 strain. (C) H3K27me2/3 ChIP-seq of *tert* (single sample; blue track) compared to WT (pooled
718 biological triplicates; black track). Sequence coverage of the *tert* ChIP input (gray track) is also
719 shown.
720
721 **Figure 5. Telomere repeats targeted to the *csr-1* locus induce an approximately 225 kb**
722 **H3K27me2/3 domain.** (A) qPCR analyses (biological triplicates) of H3K27me2/3 ChIP with
723 strains containing 8 or 17 telomere repeats at the *csr-1* locus, with WT strain as a control
724 (means displayed; error bars show standard deviation; asterisks represent $p<0.05$ and $p<0.01$
725 respectively). Level of H3K27me2/3 normalized to Telomere 1L. (B) H3K27me2/3 ChIP-seq of
726 full WT LG I (pooled biological triplicates; black track). Black circle indicates the centromere, *csr-*

1 position is indicated by vertical line, and arrows at chromosome ends indicate 5' to 3' polarity of telomere repeats. Expansion below shows the extent and shape of the H3K27me2/3 domain induced in the Δ*csr-1*::$(TTAGGG)_{17}$ strain (single sample; green track) compared to WT (black track). Site of *csr-1* replacement with telomere repeats indicated below ChIP-seq tracks. Genes are displayed as black bars.

Figure S1. Three kilobase segments from a natural H3K27me2/3 domain are insufficient to trigger *de novo* H3K27me2/3 at ectopic loci. (A) Distribution of H3K27me2/3 (black), genes (gray) and H3K9me3 (blue, inverted) are displayed for the left subtelomere of LG VI (Jamieson et al. 2013). The red bar indicates the region deleted for the transplantation experiments. The eight three kb segments (expanded below the black bar) were targeted to the *his-3* and *csr-1* loci. Green vertical bars represent the locations of qPCR primer pairs used in H3K27me2/3 ChIP experiments. H3K27me2/3 ChIP-qPCR indicates the absence of ectopic H3K27me2/3 in strains containing regions 1-8, each separately targeted to (B) *his-3* and (C) *csr-1*. Each ChIP experiment was performed in biological triplicate; qPCR analyses were performed on each sample in technical triplicate. Bars represent means of biological triplicates and error bars show standard deviation. Primers are listed in Table S2.

Figure S2. qPCR validation of H3K27me2/3 ChIP-seq data from translocation strains. The gains and losses of H3K27me2/3 in ChIP-seq experiments were confirmed by ChIP-qPCR at representative regions for UK3-41 (A), OY350 (B), ALS159 (C), OY329 (D), NM149 (E), OY337 (F), UK2-32 (G), and AR16 (H). Each ChIP experiment was performed in biological triplicate; qPCR analyses were performed on each sample in technical triplicate. Bars represent means of biological triplicates and error bars show standard deviation. Primers are listed in Table S2.

Figure S3. qPCR validation of RNA-seq expression changes in translocation OY350. The effects of gain of H3K27me2/3 (A) and loss of H3K27me2/3 (B,C) on associated gene expression levels were verified by qPCR. Gene expression levels were normalized to housekeeping gene, NCU02840. qPCR analyses were performed on each sample in technical triplicate. Bars

represent means of biological triplicates and error bars show standard deviation. Primers are listed in Table S2.

Figure S4. H3K27me2/3 profiles of additional strains containing chromosomal rearrangements. Chromosome rearrangements and H3K27me2/3 ChIP-seq (pooled biological triplicates) profiles are shown for translocations UK2-32 (A), AR16 (B) and OY337 (C). Magenta curved arrows illustrate the movement of chromosomal segments in the translocations. Blue and dashed lines distinguish chromosome sources while arrows indicate the directionality of translocated segments. Light gray lines highlight regions of uncertainty with respect to the locations of breakpoints based on available genetic evidence (see Methods). Solid red line indicates chromosome deletions. H3K27me2/3 ChIP-seq tracks of WT and translocation strains are displayed above chromosome diagrams. H3K27me2/3 that was lost in a translocation strain is highlighted in orange in the corresponding WT track while new H3K27me2/3 is indicated in green. Conserved H3K27me2/3 is shown in black. Circles indicate centromeres. Dark gray bars indicate 500 kb.

Figure S5. Whole genome view of H3K27me2/3 ChIP-seq in WT and *tert*. H3K27me2/3 ChIP-seq for all seven *N. crassa* chromosomes is displayed for WT (pooled biological triplicates; black track) and *tert* (single sample; blue). The y-axis is number of reads averaged over 25 bp windows. Open black or blue circles indicate location of centromeres.

778 **Table S1. List of strains**

Strain	Genotype
N51 (FGSC 2225)	*mat A;* Mauriceville
N625	*mat a; his-3*
N2931	*mat a;* Δ*mus-52::bar*$^{+}$
N3752 (FGSC 2489)	*mat A;* Oak Ridge
N4730	*mat A;* Δ*set-7::bar*$^{+}$
N4933	*mat a*; Δ47.4 kb::*hph*$^{+}$
N5100 (FGSC 1614)	*mat a;* In(IL->IR)AR16
N5101 (FGSC 2100)	*mat A;* T(IV->VI)ALS159
N5102 (FGSC 3670)	*mat A;* T(VI->III)OY329
N5547	*mat a;* Δ*mus-52::bar*$^{+}$*;* Δ47.4 kb::*hph*$^{+}$
N5683	*mat A*; *his-3*$^{+}$*::1;* Δ47.4 kb::*hph*$^{+}$
N5684	*mat A*; *his-3*$^{+}$*::2;* Δ47.4 kb::*hph*$^{+}$
N5685	*mat A*; *his-3*$^{+}$*::3;* Δ47.4 kb::*hph*$^{+}$
N5686	*mat A*; *his-3*$^{+}$*::4;* Δ47.4 kb::*hph*$^{+}$
N5687	*mat A*; *his-3*$^{+}$*::5;* Δ47.4 kb::*hph*$^{+}$
N5688	*mat A*; *his-3*$^{+}$*::6;* Δ47.4 kb::*hph*$^{+}$
N5689	*mat A*; *his-3*$^{+}$*::7* Δ47.4 kb::*hph*$^{+}$
N5690	*mat A*; *his-3*$^{+}$*::8;* Δ47.4 kb::*hph*$^{++}$
N5695	*mat a*; Δ*csr-1::1;* Δ47.4 kb::*hph*$^{+}$
N5696	*mat a*; Δ*csr-1::2;* Δ47.4 kb::*hph*$^{+}$
N5697	*mat a*; Δ*csr-1::3;* Δ47.4 kb::*hph*$^{+}$
N5698	*mat A*; Δ*csr-1::4;* Δ47.4 kb::*hph*$^{+}$
N5699	*mat A*; Δ*csr-1::5;* Δ47.4 kb::*hph*$^{+}$

N5700	*mat a*; Δ*csr-1::6;* Δ47.4 kb::*hph*$^+$
N5701	*mat a*; Δ*csr-1::7;* Δ47.4 kb::*hph*$^+$
N5702	*mat A*; Δ*csr-1::8;* Δ47.4 kb::*hph*$^+$
N5739	*mat A*; *his-3;* Δ47.4 kb::*hph*$^+$
N5857 (FGSC 1483)	*mat A;* T(II->V)NM149
N5858 (FGSC 3668)	*mat A;* T(II->IV)OY337, *al-2*
N5859 (FGSC 7294)	*mat A;* T(IVR->VL)UK2-32
N5862 (FGSC 4641)	*mat A;* T(VIL->IR)OY350
N5863 (FGSC 3635)	*mat A;* T(VI->III)OY320
N5865 (FGSC 2643)	*mat A;* T(II->III)AR16
N5866 (FGSC 6869)	*mat A; inl*; T(VR)UK3-41
N6089	*mat a;* Dp(VI->III)OY329
N6093 (FGSC 3671)	*mat a;* T(VI->III)OY329
N6228	*mat A;* Δ*tert::nat-1*$^+$
N6381	*mat a;* Δ*mus-52::bar*$^+$*;* Δ*csr-1::*$(TTAGGG)_8$
N6383	*mat a;* Δ*mus-52::bar*$^+$*;* Δ*csr-1::*$(TTAGGG)_{17}$
N6984	*mat a;* Δ*mus-52::bar*$^+$*;* Δ*csr-1::*$(TTAGGG)_8$
N6985	*mat a;* Δ*mus-52::bar*$^+$*;* Δ*csr-1::*$(TTAGGG)_8$
N6986	*mat a;* Δ*mus-52::bar*$^+$*;* Δ*csr-1::*$(TTAGGG)_{17}$
N6987	*mat a;* Δ*mus-52::bar*$^+$*;* Δ*csr-1::*$(TTAGGG)_{17}$

783 **Table S2. List of primers**

784

Primer	Description	Sequence
3325	Construction of *his-* 3^{+}*::1* (N5683)	CGGGATCCCCGGATCGAACGGCGGATGG (BamHI)
3326	Construction of *his-* 3^{+}*::1* (N5683)	GCTCTAGATGAGCTCCTTCCCCCACGGT (XbaI)
3327	Construction of *his-* 3^{+}*::2* (N5684)	CGGGATCCCGTGGGTTCCAGTGCGTCCC (BamHI)
3328	Construction of *his-* 3^{+}*::2* (N5684)	GCTCTAGATGGCAAGCGCCGACATGTGA (XbaI)
3329	Construction of *his-* 3^{+}*::3* (N5685)	GGGCCCAGGGAACAGGCGCAGTGCAG (ApaI)
3330	Construction of *his-* 3^{+}*::3* (N5685)	GACTAGTTGGCGCGCTTGACCAGCAAA (SpeI)

3331	Construction of *his- 3^{+}::4* (N5686)	GACTAGTTCCCGGAACGGCCACTCCAT (SpeI)
3332	Construction of *his- 3^{+}::4* (N5686)	GCTCTAGAGTGCTGCCAAGGCCCGACAT (XbaI)
3297	Construction of *his-3^{+}::5* (N5687)	GGAATTCCAAAGGATCGCGCCCGGAGG (EcoRI)
3333	Construction of *his-3^{+}::5* (N5687)	CGGGATCCACGACGGGAAGACGAGGGGT (BamHI)
3334	Construction of *his- 3^{+}::6* (N5688)	GGGCCCGGGAGTGTGGCGCTGTGGAC (ApaI)
3335	Construction of *his- 3^{+}::6* (N5688)	GACTAGTAGCAGCATCTCGGGTCCGGT (SpeI)
3301	Construction of *his- 3^{+}::7* (N5689)	GGAATTCGGCATGCCCAGGGATTGGGG (EcoRI)
3336	Construction of *his- 3^{+}::7* (N5689)	GCTCTAGAGACGGAACGGTGACAGGCGG (XbaI)
3303	Construction of *his- 3^{+}::8* (N5690)	GGAATTCTGGTTCGCGGACGAGGGCTA (EcoRI)
3337	Construction of *his- 3^{+}::8* (N5690)	CGGGATCCGGCTATTGCTGCCAGCCGGT (BamHI)
4654	3' *csr-1* RP	AACACCTCCGTCGCCATAAACTCC
4655	5' *csr-1* FP	GGCCCCTGGTTTACTGAGGGC
4721	5' *csr-1* RP	TGCAGCCATTGACGACATTGC
4722	3' *csr-1* FP	TGGATTTCCTGCGCTGCACAC
4723	Construction of Δ*csr-1::1* (N5695)	GCAATGTCGTCAATGGCTGCACCGGATCG AACGGCGGATGG
4724	Construction of Δ*csr-1::1* (N5695)	GTGTGCAGCGCAGGAAATCCATGAGCTCC TTCCCCCACGGT

4725	Construction of Δ*csr-1::2* (N5696)	GCAATGTCGTCAATGGCTGCACGTGGGTTCCAGTGCGTCC
4726	Construction of Δ*csr-1::2* (N5696)	GTGTGCAGCGCAGGAAATCCATGGCAAGCGCCGACATGTGA
4727	Construction of Δ*csr-1::3* (N5697)	GCAATGTCGTCAATGGCTGCAAGGGAACAGGCGCAGTGCAG
4728	Construction of Δ*csr-1::3* (N5697)	GTGTGCAGCGCAGGAAATCCATGGCGCGCTTGACCAGCAAA
4729	Construction of Δ*csr-1::4* (N5698)	GCAATGTCGTCAATGGCTGCATCCCGGAACGGCCACTCCAT
4730	Construction of Δ*csr-1::4* (N5698)	GTGTGCAGCGCAGGAAATCCAGTGCTGCCAAGGCCCGACAT
4731	Construction of Δ*csr-1::5* (N5699)	GCAATGTCGTCAATGGCTGCACAAAGGATCGCGCCCGGAGG
4732	Construction of Δ*csr-1::5* (N5699)	GTGTGCAGCGCAGGAAATCCAACGACGGGAAGACGAGGGGT
4733	Construction of Δ*csr-1::6* (N5700)	GCAATGTCGTCAATGGCTGCAGGGAGTGTGGCGCTGTGGAC
4734	Construction of Δ*csr-1::6* (N5700)	GTGTGCAGCGCAGGAAATCCAAGCAGCATCTCGGGTCCGGT
4735	Construction of Δ*csr-1::7* (N5701)	GCAATGTCGTCAATGGCTGCAGGCATGCCCAGGGATTGGGG
4736	Construction of Δ*csr-1::7* (N5701)	GTGTGCAGCGCAGGAAATCCAGACGGAACGGTGACAGGCGG
4737	Construction of Δ*csr-1::8* (N5702)	GCAATGTCGTCAATGGCTGCATGGTTCGCGGACGAGGGCTA
4738	Construction of Δ*csr-1::8* (N5702)	GTGTGCAGCGCAGGAAATCCAGGCTATTGCTGCCAGCCGGT
4784	qChIP *his-3* & *csr-1* targeting P1Fwd	AATGCAAGGTCCCGAACACT
4785	qChIP *his-3* & *csr-1* targeting P1Rev	TGGCTGTCGCAATTACCAGT

4786	qChIP *his-3* & *csr-1* targeting P2Fwd	GACCAAGCATGCGTTAGCTG
4787	qChIP *his-3* & *csr-1* targeting P2Rev	ACCCAAGGTGGGTGTGTTTT
4788	qChIP *his-3* & *csr-1* targeting P3Fwd	CCGTTTGAGCTGGTCTTCCT
4789	qChIP *his-3* & *csr-1* targeting P3Rev	TGACGGATGCTCTTTGTCCC
4790	qChIP *his-3* & *csr-1* targeting P4Fwd	CAACCAGCTTGACGGCTTTC
4791	qChIP *his-3* & *csr-1* targeting P4Rev	TACCGTAGGTGCCCTGTGTA
3317	qChIP *his-3* & *csr-1* targeting P5Fwd and deletion analysis	CCCCTTCCTGCCGTGGGAGA
3562	qChIP *his-3* & *csr-1* targeting P5Rev and deletion analysis	TCAGCAGGCATAGTCAAGACTGGT
4782	qChIP *his-3* & *csr-1* targeting P6Fwd	CCCGCTTCAGCAACCAAGTT
4783	qChIP *his-3* & *csr-1* targeting P6Rev	AACTTTAGCCCGCGTTACGG
3319	qChIP *his-3* & *csr-1* targeting P7Fwd and deletion analysis	TGGGTCGATGGAGTACCTTCCCC
3563	qChIP *his-3* & *csr-1* targeting P7Rev and deletion analysis	TGCACTATCCTTTTCAGGGGCTTGT
3902	qChIP *his-3* & *csr-1* targeting P8Fwd	GACCTACACGGCCCGGGGAA
3903	qChIP *his-3* & *csr-1* targeting P8Rev	ACCGACGAGACTTGACTGCCCA
3986	qChIP *his-3* & *csr-1* targeting P9Fwd	GTGGCGGCGTGAACGGTCAT
3987	qChIP *his-3* & *csr-1* targeting P9Rev	AGTCAAGCCTCGCGATCGTGA
3321	qChIP *his-3* & *csr-1* targeting P10Fwd	TGAACAGGTGACGGCGGGAGT

3564	qChIP *his-3* & *csr-1* targeting P10Rev	CGGGTCCGGAGTCCATCACCA
3976	qChIP *his-3* & *csr-1* targeting P11Fwd	AGTGGTCCAGAGTGGGATCGGT
3977	qChIP *his-3* & *csr-1* targeting P11Rev	ACCGCCAATATGGCATCGCCC
3974	qChIP *his-3* & *csr-1* targeting P12Fwd	TGACGGCGCGCAGATTGGAG
3975	qChIP *his-3* & *csr-1* targeting P12Rev	TCGCTTCCCTTCTCCCACCATCC
3978	qChIP *his-3* & *csr-1* targeting P13Fwd	TTGACGGCGCGCAGATTGGAG
3979	qChIP *his-3* & *csr-1* targeting P13Rev	CCACCATCCTTCCCTCTGCCACA
3992	qChIP *his-3* & *csr-1* targeting P14Fwd	CATCGCAGCTCAACCGCAGA
3993	qChIP *his-3* & *csr-1* targeting P14Rev	GCCAGCCGGTGTCAAGACAGA
3904	qChIP *his-3* & *csr-1* targeting P15Fwd	AACAAAGACGCTCTTCTGGTGGCC
3905	qChIP *his-3* & *csr-1* targeting P15Rev	ACTACCAAACTGCCGACGGCT
3943	Construction of Δ47.4 kb::*hph*$^{+}$(N4933)	GTAACGCCAGGGTTTTCCCAGTCACGACGT GTGGCTTGCAGGCACGCAA
3944	Construction of Δ47.4 kb::*hph*$^{+}$(N4933)	ACCGGGATCCACTTAACGTTACTGAAATCA GTCCGAGTGGGCCTGCCTC
3945	Construction of Δ47.4 kb::*hph*$^{+}$(N4933)	GCTCCTTCAATATCATCTTCTGTCGACGGAC CACCACCCAGCGTGGAAAG
3946	Construction of Δ47.4 kb::*hph*$^{+}$(N4933)	GCGGATAACAATTTCACACAGGAAACAGCT TGCCGCCGGCTGAGAAACC
4960	ALS159 (N5101) qPCR	TTGGGATGATTTGGGACGGG
4961	ALS159 (N5101) qPCR	TCCCAAGCTGACAGTTCCAC

4961	ALS159 (N5101) qPCR	TGCATGCTCTCCCCCTTTTG
4963	ALS159 (N5101) qPCR	TCTGAGGGATGTGCCAAACC
4974	NM149 (N5857) qPCR	CGCCATTTCTACCCCGATGA
4975	NM149 (N5857) qPCR	TGCCAAGCCATCTTTTTGCC
4976	NM149 (N5857) qPCR	CTACGGGTTGCTGCCAAGTA
4977	NM149 (N5857) qPCR	CCTCAGAGAATCGGGGCATC
4978	NM149 (N5857) qPCR	GGGCTCAGTCACTTGCTACA
4979	NM149 (N5857) qPCR	GATATACCCGCACCAGCACA
4984	OY337 (N5858) qPCR	CTTCGCCTCTCACTCCGATG
4985	OY337 (N5858) qPCR	GGCAGCTAGCAATCGGTTTT
4986	OY337 (N5858) qPCR	GAGCCTGTCCAAGACGACAA
4987	OY337 (N5858) qPCR	CGGTGACGGTAGTGTGTAGG
4990	OY337 (N5858) qPCR	GTTACTGGCGGGAAATGGGA
4991	OY337 (N5858) qPCR	TTGGGACCAGGTTTGTCCAC
4996	OY350 (N5862) qPCR	GCCTTGGACCCTCGAATGAA
4997	OY350 (N5862) qPCR	TGGGAAAACGTGGGGGAAAA
4998	OY350 (N5862) qPCR	TGGGTGAGGTCTTTGGAGGA
4999	OY350 (N5862) qPCR	AAGAGTTCCTGAACGTCGCC
5002	OY350 (N5862) qPCR	AGGGTTGCTGGTAATCCGTG

5003	OY350 (N5862) qPCR	CAAGGCTTGGGGAAAGGGAA
3317	UK3-41 (N5866) qPCR	CCCCTTCCTGCCGTGGGAGA
3562	UK3-41 (N5866) qPCR	TCAGCAGGCATAGTCAAGACTGGT
3954	UK3-41 (N5866) qPCR	GTAGCTAGCGGGTGCTGCCG
3955	UK3-41 (N5866) qPCR	AGGCGCCAGGAAGAGTATAGCCC
5012	OY329 (N5102) qPCR	AAATCCACTCATCCTCGGCG
5013	OY329 (N5102) qPCR	CTCGGATCACCGTCAACAGG
5020	OY329 (N5102) qPCR	ATGGTAACGTGGACAGGTGC
5021	OY329 (N5102) qPCR	TTGAACGCCGTAGAGGGATG
5028	UK2-32 (N5859) qPCR	AGGAAGTACGCCTTGCAGTC
5029	UK2-32 (N5859) qPCR	CCTGTATAATGGCGGTCCCC
5034	UK2-32 (N5859) qPCR	TCGAACCATGTGAGCTGCTT
5035	UK2-32 (N5859) qPCR	GAGAACGCCGAATCGCTCTA
5036	AR16 (N5100) qPCR	GAGAACGCCGAATCGCTCTA
5037	AR16 (N5100) qPCR	GCCCCCTTTTTGTCGTTAGC
5040	AR16 (N5100) qPCR	CGTCAACGGTAGCTGGAAGA
5041	AR16 (N5100) qPCR	CCTCTTTGTGTCGAAGCCCA
5042	AR16 (N5100) qPCR	TGCCAAAGCACAACAAGCTG
5043	AR16 (N5100) qPCR	TTGATACCACGGGCTTCGAC

5046	AR16 (N5100) qPCR	GGATCATCGGTAGGTTGGGT
5047	AR16 (N5100) qPCR	TCAGATCCAGCTAGTTTCGCC
5316	Telomere repeat FP	TTAGGGTTAGGGTTAGGG
5317	Telomere repeat RP	CCCTAACCCTAACCC
5318	Targeting tel repeats to *csr-1* FP1	GCAATGTCGTCAATGGCTGCAATTAACCCTCACTAAAGGGA
5319	Targeting tel repeats to *csr-1* RP1	GTGTGCAGCGCAGGAAATCCATAATACGACTCACTATAGGG
5320	Targeting tel repeats to *csr-1* FP2	GTGTGCAGCGCAGGAAATCCAATTAACCCTCACTAAAGGGA
5321	Targeting tel repeats to *csr-1* RP2	GCAATGTCGTCAATGGCTGCATAATACGACTCACTATAGGG
5322	Verify LG I circularization FP	AGAGGAGTCCGTAGGCGAAT
5323	Verify LG I circularization RP	TCGTTCGGTTGACAGCTTGA
5324	Verify LG II circularization FP	TGTTTCGGCGATGGGAAGAA
5325	Verify LG II circularization RP	ACTTCGAGTATGTAGCGGCG
5326	Verify LG III circularization FP	CGAGGCTCCATAATGCTCGT

5327	Verify LG III circularization RP	TATTATAGGGCGCGCGGAAG
5328	Verify LG IV circularization FP	GGCGCAAAAACCTTCCTACC
5329	Verify LG IV circularization RP	ACGACAGGGCCTAGGGTAAT
5330	Verify LG VI circularization FP	TAGGTTGAAGGCTATCGGCG
5331	Verify LG VI circularization RP	CCTTGGTTGCATTTGGTGGG
5332	Verify LG VII circularization FP	GCCTTCGGCTACCTTTCCTT
5346	Verify LG VII circularization RP	CTCCCTTTCAGCTCGTGTGT
5353	3' *csr-1* qPCR FP	CGCCGTTAATGCAGTTGTGAT
5354	3' *csr-1* qPCR RP	CCCCAGCAACTGCGTCTATT
5133	NM149 (N5857) breakpoint 1 FP	TTGCGGCAAGTTTGAAGTCG
5134	NM149 (N5857) breakpoint 1 RP	TGAAGCGTAAGCTCGTGTGT
5130	NM149 (N5857) breakpoint 2 FP	GCTCAAAGTGGGGACTGACA
5154	NM149 (N5857) breakpoint 2 RP	ATCCTTCTCCGCTGTTTCGG

5123	OY329 (N5102) breakpoint 1 FP	GTTGTTGTGGTTTCCTCGCC
5124	OY329 (N5102) breakpoint 1 RP	ATATAGGCGTAGCGTTGCCC
5125	OY329 (N5102) breakpoint 2 FP	TGTTGCCTGGACTGCTAGTG
5126	OY329 (N5102) breakpoint 2 RP	AGCCTAAACCTCGGCTAGGA
5127	OY329 (N5102) breakpoint 3 FP	CCGGTATCACGAGCTTCTCC
5128	OY329 (N5102) breakpoint 3 RP	GGGCGGAAGTTGAGCTGTAT
5155	UK3-41 (N5866) breakpoint 1 FP	GAACGGGACGTTCAAGGCTA
5157	UK3-41 (N5866) breakpoint 1 RP	TGCTTGTCTCGTTTTGCAGC
5158	UK3-41 (N5866) breakpoint 2 FP	CGGGAGAGGGGGATAGTTGA
5473	UK3-41 (N5866) breakpoint 2 RP	CGCACTCACATGCTGCATAC
5156	UK3-41 (N5866) breakpoint 3 FP	AAGGCGTAATGGACACGAGG
5472	UK3-41 (N5866) breakpoint 3 RP	GCATCGTATTTGCACCGTCC
5476	ALS159 (N5101) breakpoint 1 FP	TCCGCAGCCGAAGTTACAAT

5477	ALS159 (N5101) breakpoint 1 RP	ACGTCACTCTCTGCCCCTAT
3902	PtrpC-nat1 FP	CAACTGATATTGAAGGAGCA
1369	nat-1 RP	GGGCATGCTCATGTAGAGCG
3406	TERT KO FP1	AGCGAACTACTACCAACTACG
3407	TERT KO RP2	CCCAAAAAATGCTCCTTCAATATCAGTTGG CATGTGAGACACTATCACG
3408	TERT KO FP3	CGCTCTACATGAGCATGCCCTGCCCCTGAA AGTCTGGTACTGGGATTGG
3409	TERT KO RP4	CTTTCACGACTACCTTCCAAG
6271	6271_NCU02840_qPCR_F	CCCTCTCAGACGAGGATATTCA
6272	6272_NCU02840_qPCR_R	GCTCTGCTGCTTCTCCTTTAT
6277	6277_NCU04720_qPCR_F	TCAGGTTGGAGGAGAGGTATAA
6278	6278_NCU04720_qPCR_R	CTATGAGGCCGAAATCCTTGT
6281	6281_NCU10030_qPCR_F	CTGCGATCGTAACACTGGATTA
6282	6282_NCU10030_qPCR_R	CCGTCCGACATGTAATTACTCAG
6283	6283_NCU10031_qPCR_F	CCGATGTCCAGAAGCAGTATATTA
6284	6284_NCU10031_qPCR_R	CAGAGCAACTGAGTGGATAGTC
3565	Telomere 1L qPCR FP	AGCGTTCAAATGCCGTGACCTGT
3566	Telomere 1L qPCR RP	AGTCCAATGGTGCTAACGGCGA

785
786

Table S3: List of plasmids

Plasmid	Description
1991	pBM61 – *his-3* targeting vector
3110	LG VIL H3K27me2/3 segment #1 cloned into 1991
3111	LG VIL H3K27me2/3 segment #2 cloned into 1991
3112	LG VIL H3K27me2/3 segment #3 cloned into 1991
3113	LG VIL H3K27me2/3 segment #4 cloned into 1991
3114	LG VIL H3K27me2/3 segment #5 cloned into 1991
3115	LG VIL H3K27me2/3 segment #6 cloned into 1991
3116	LG VIL H3K27me2/3 segment #7 cloned into 1991
3117	LG VIL H3K27me2/3 segment #8 cloned into 1991
3172	$(TTAGGG)_{76}$ cloned into pCR4-TOPO-TA
FGSC #10598	pAL12-Lifeact – source of *trpC::nat-1*

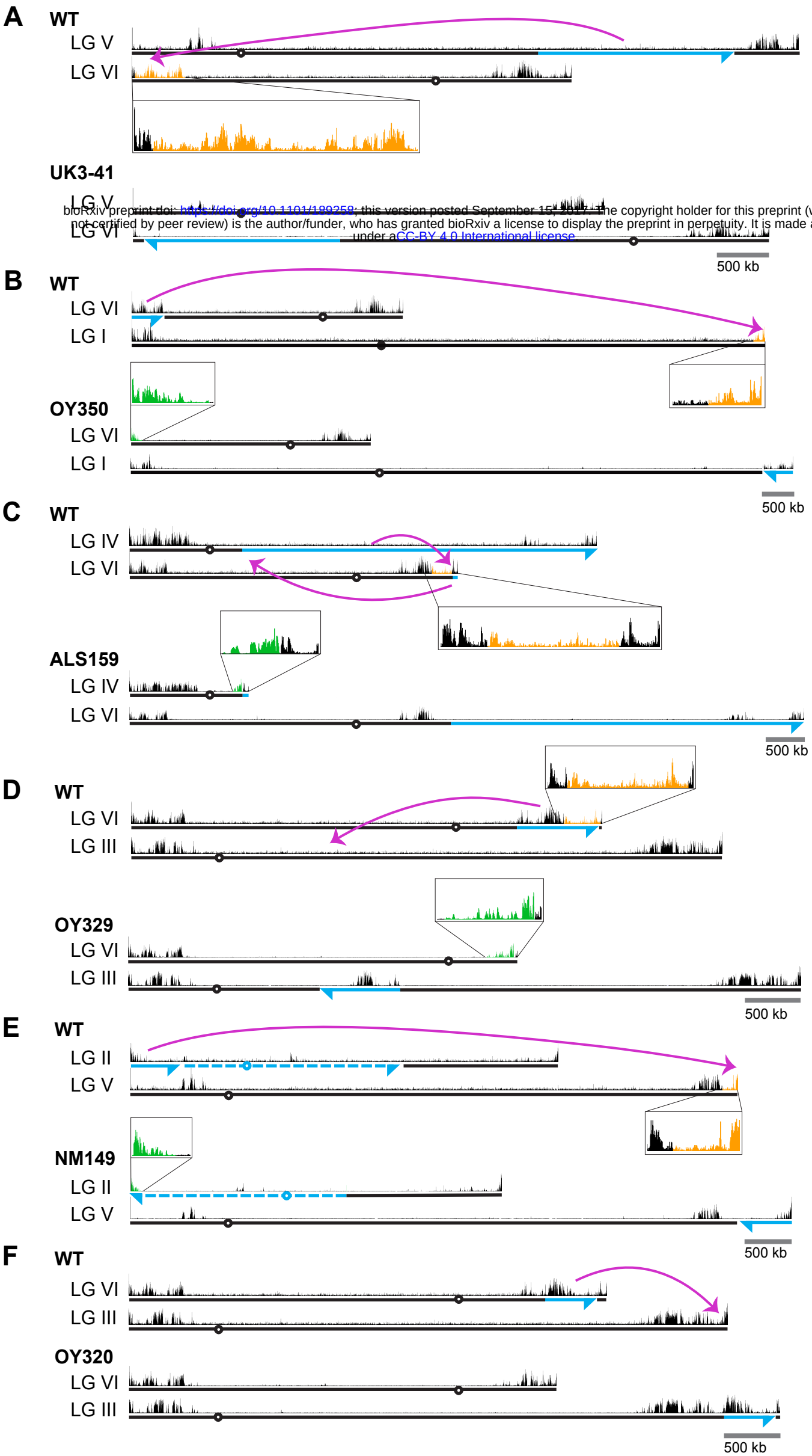

Jamieson_Fig2

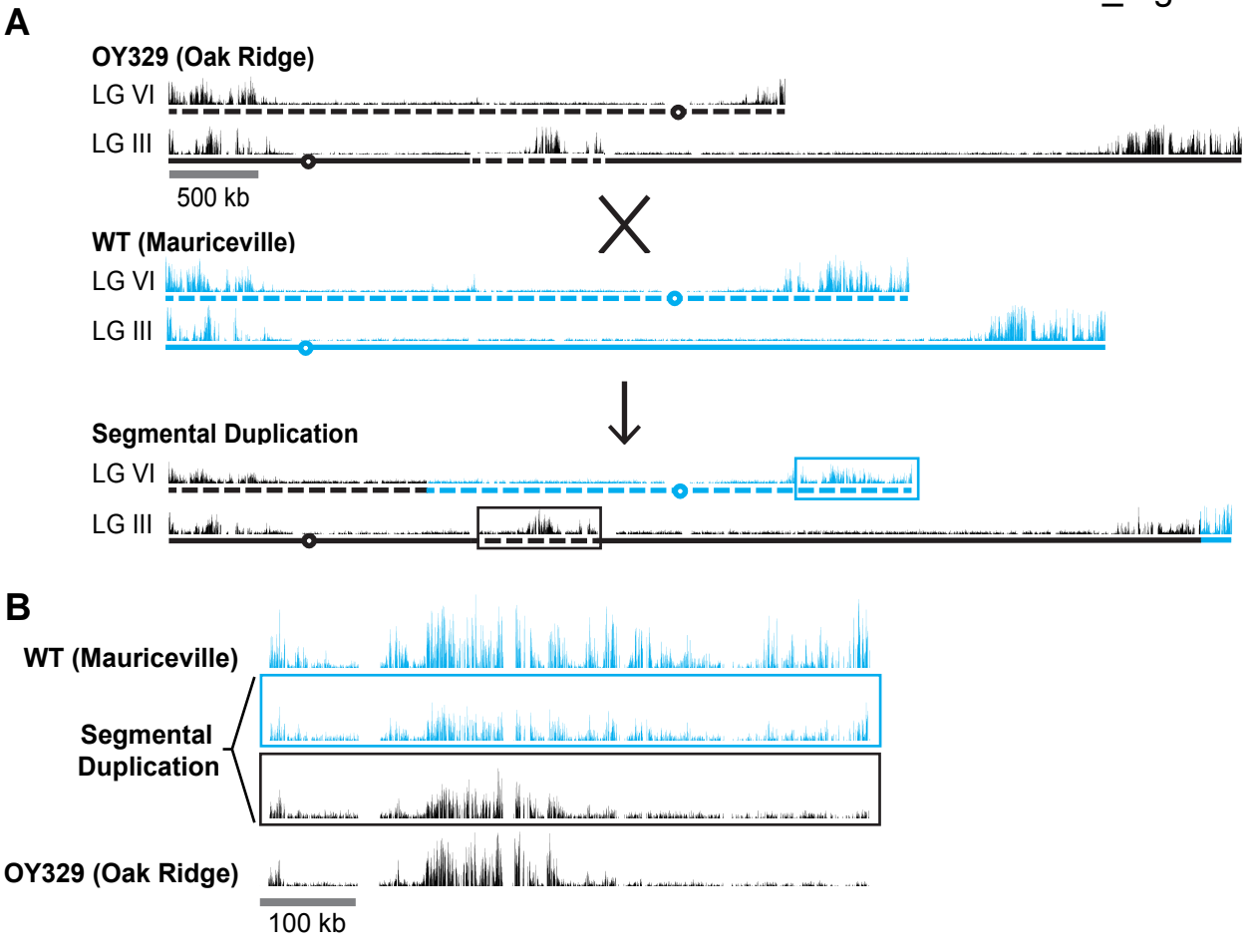

Jamieson_Fig3

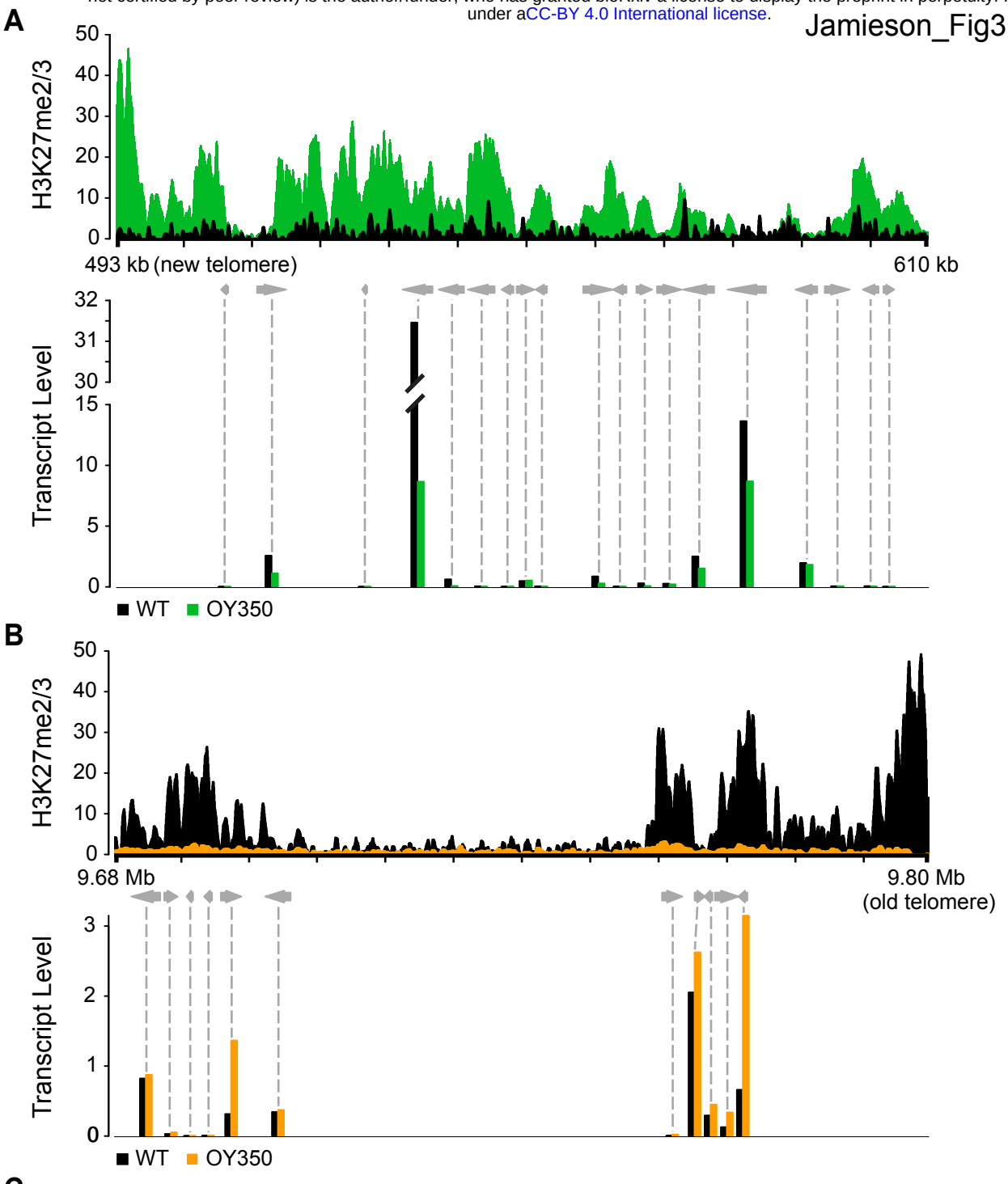

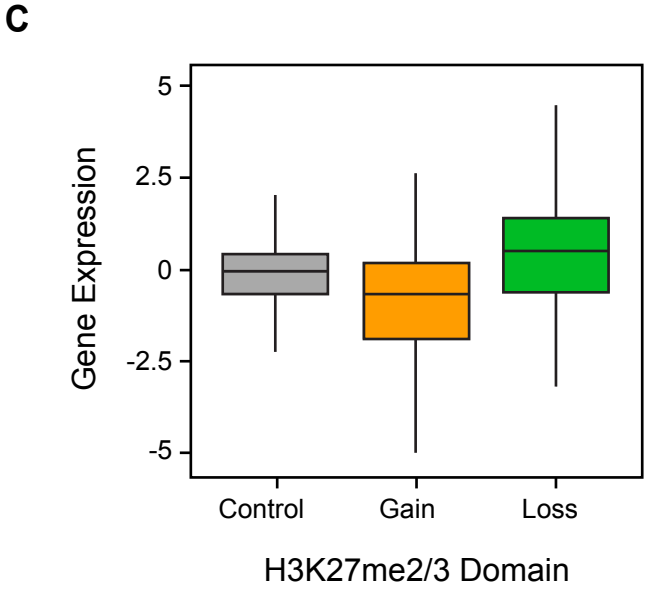

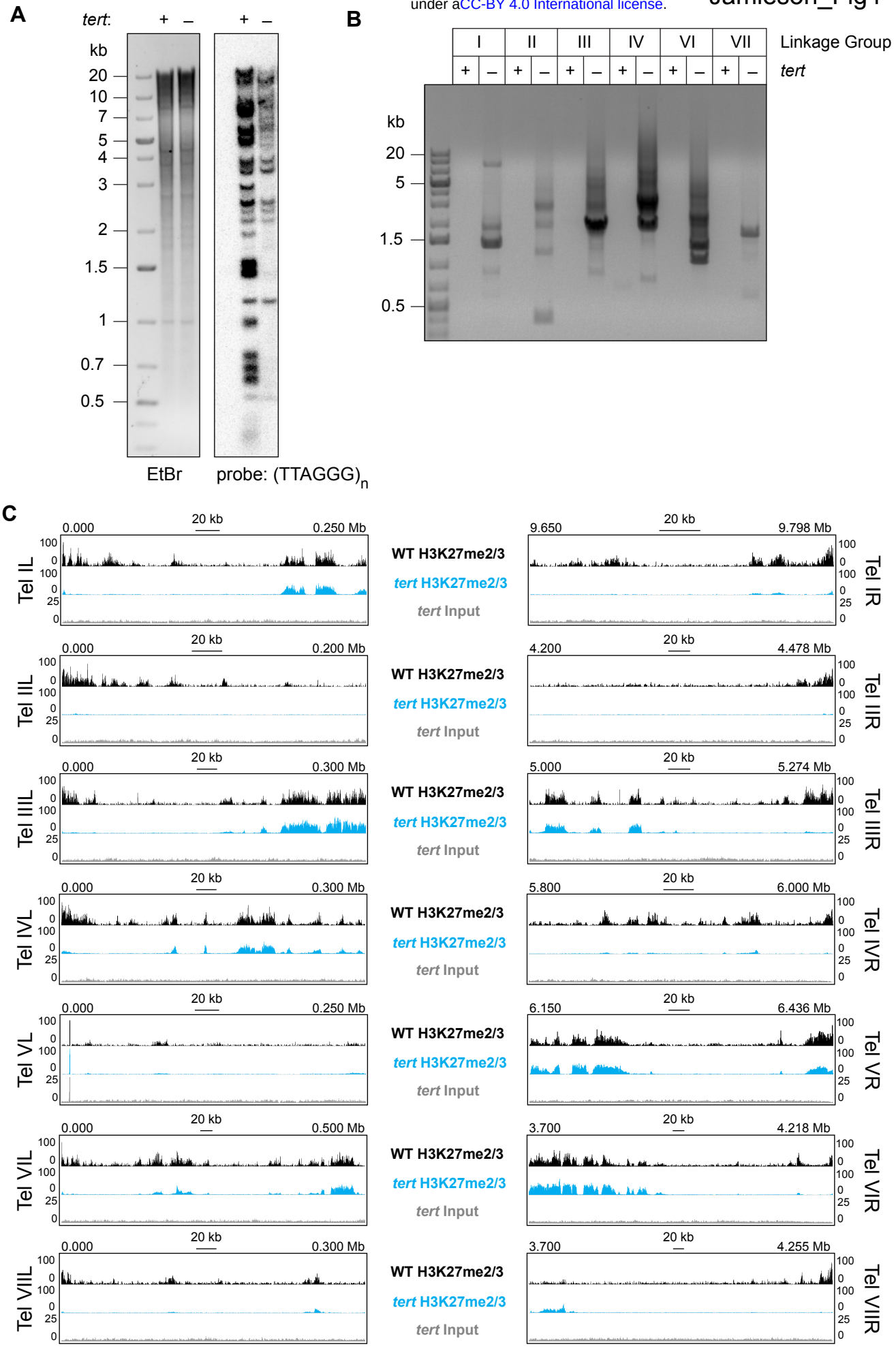

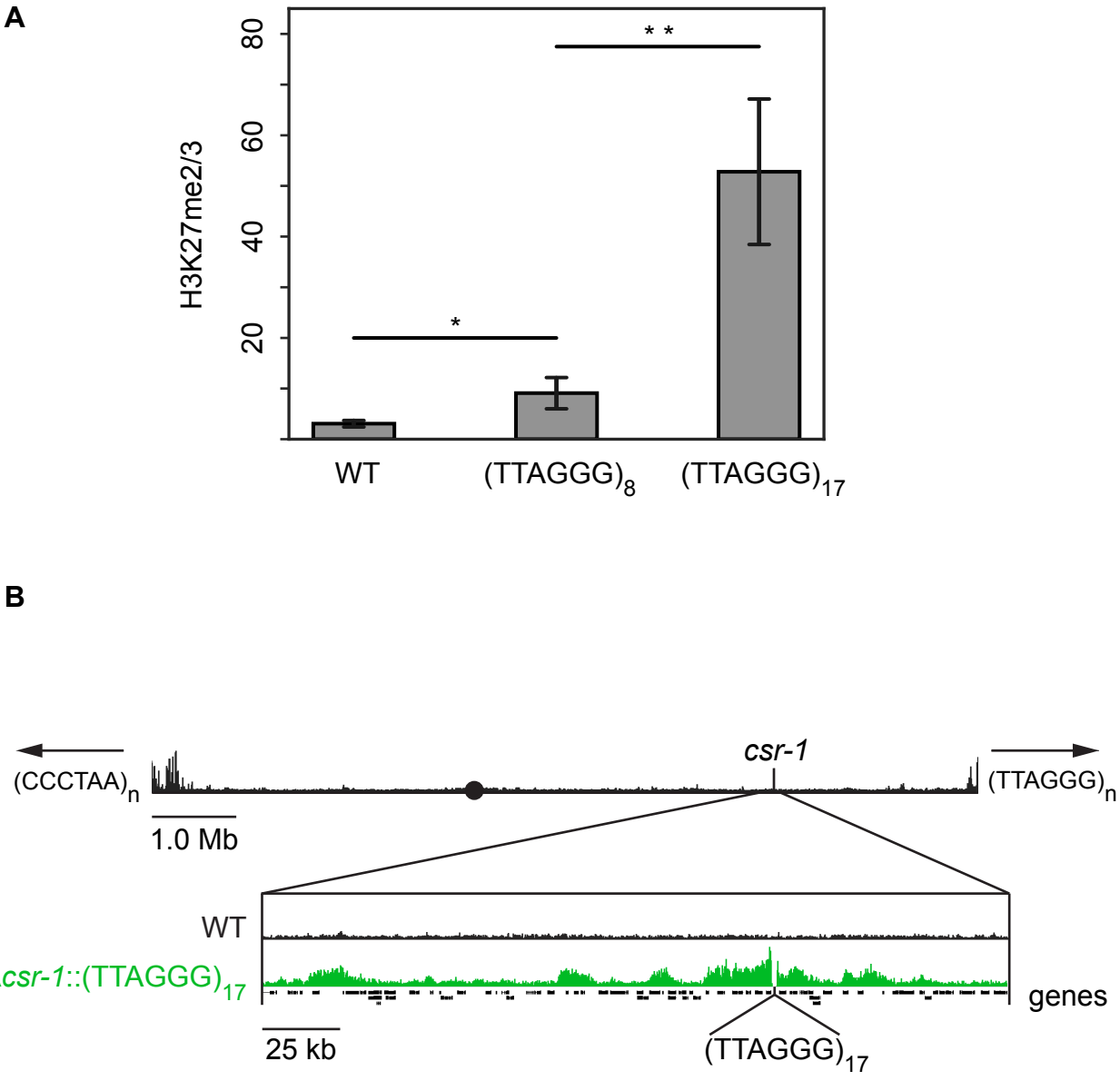

Jamieson_FigS1A

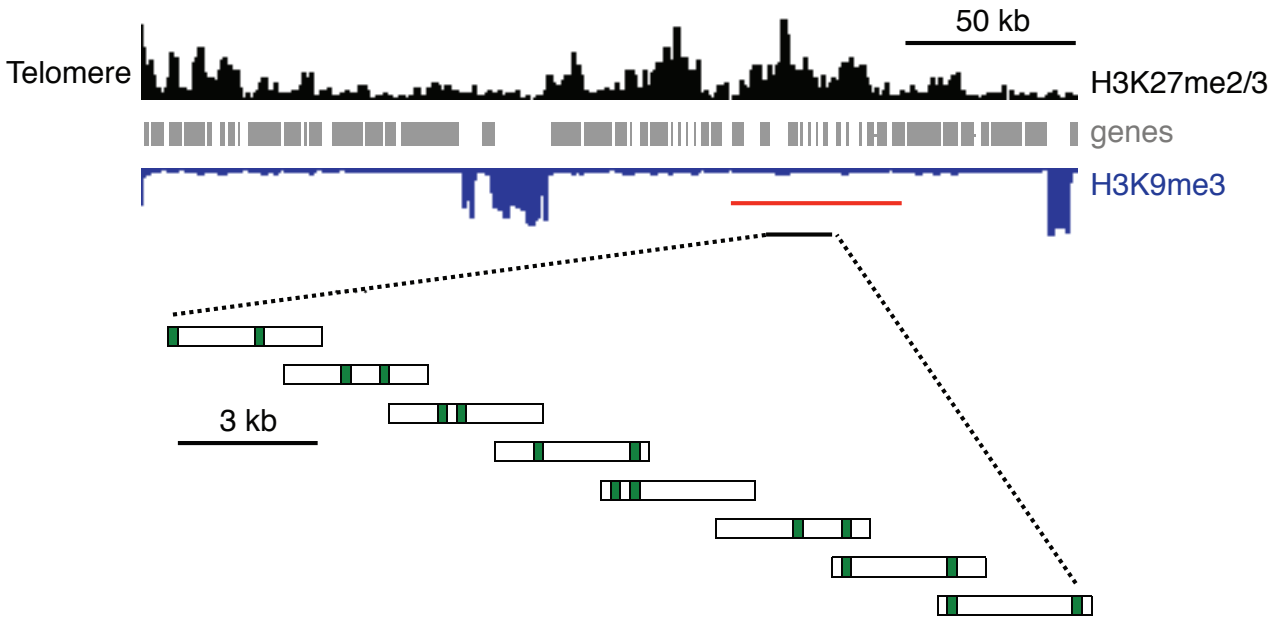

B

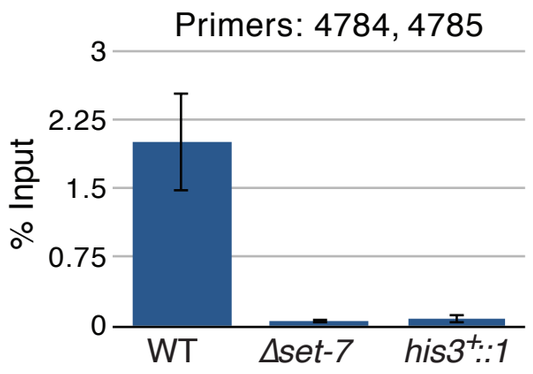

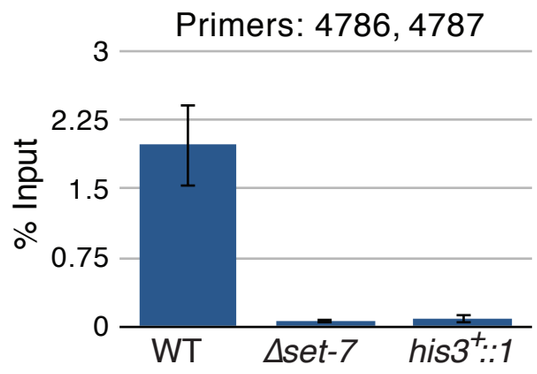

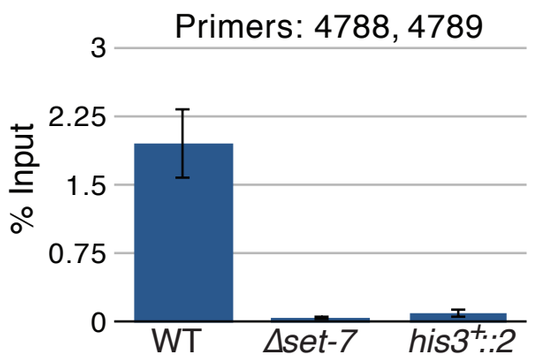

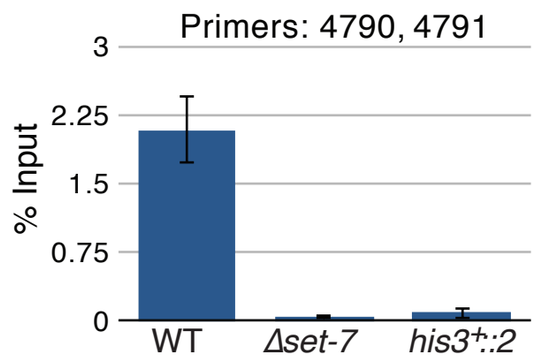

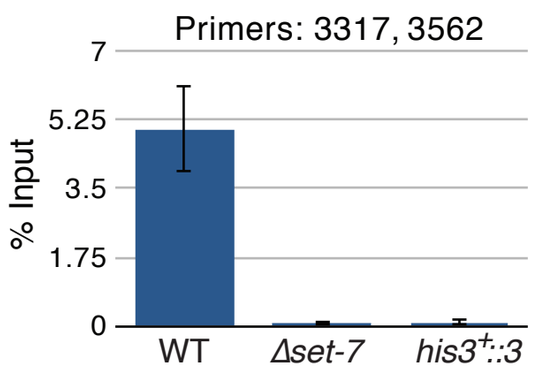

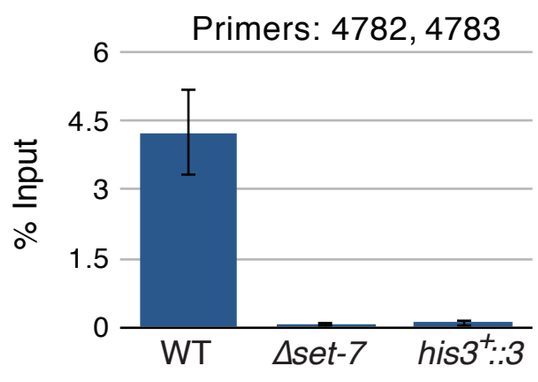

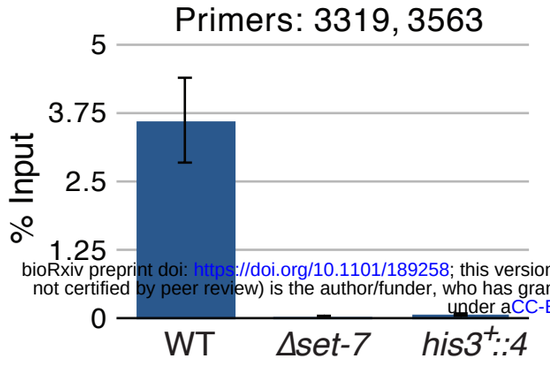

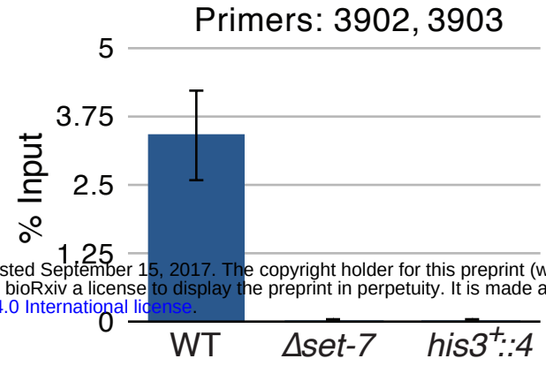

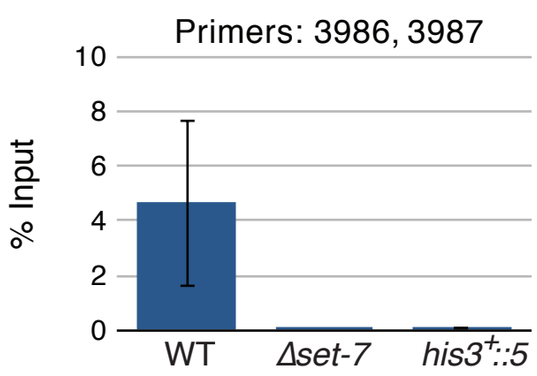

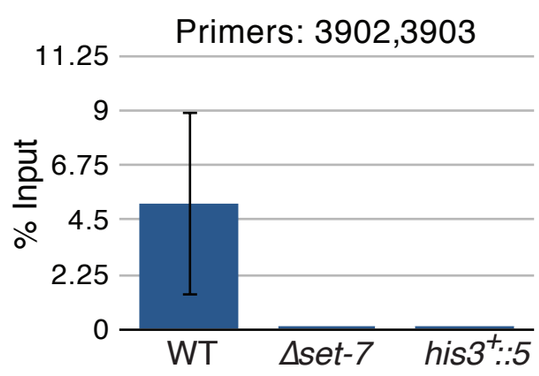

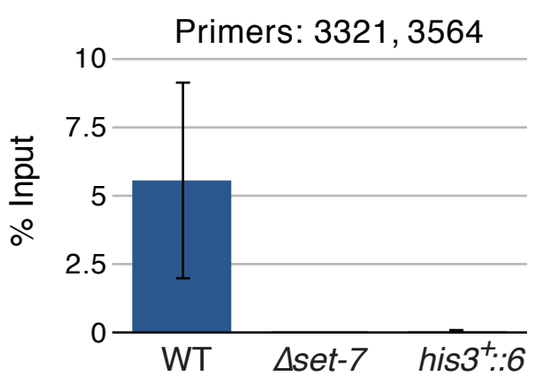

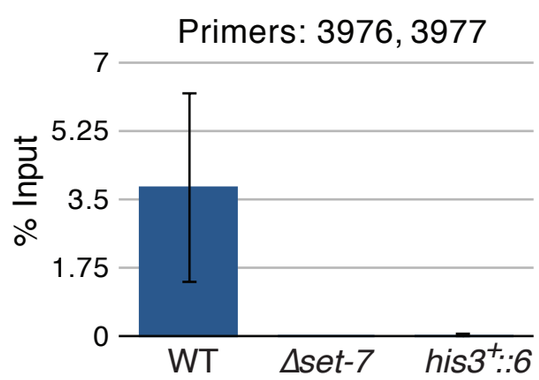

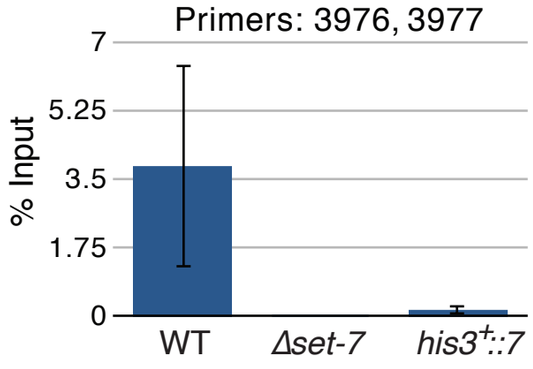

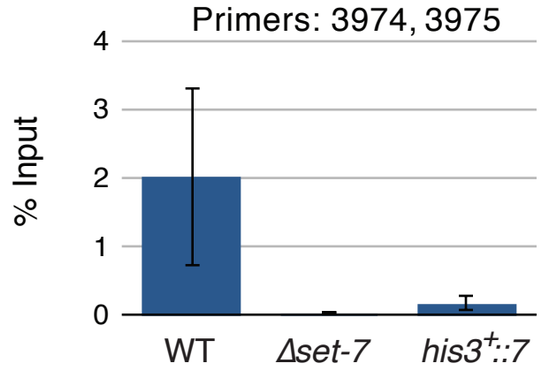

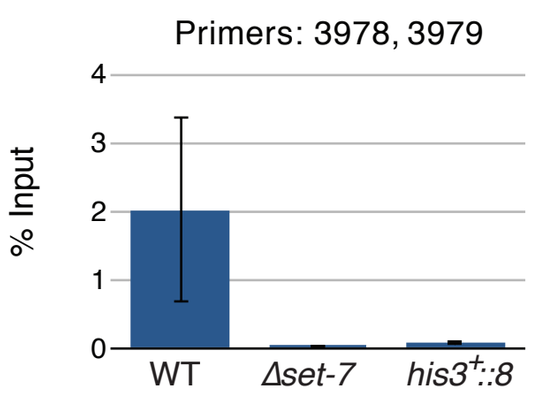

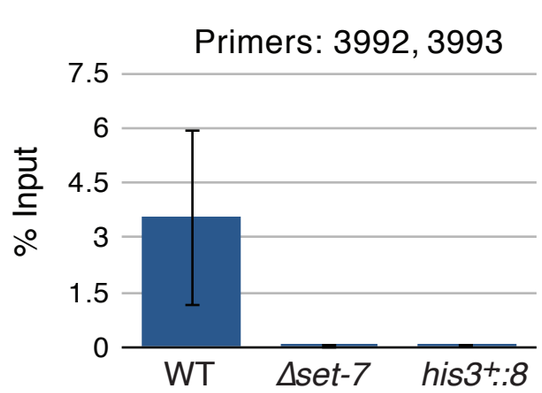

C

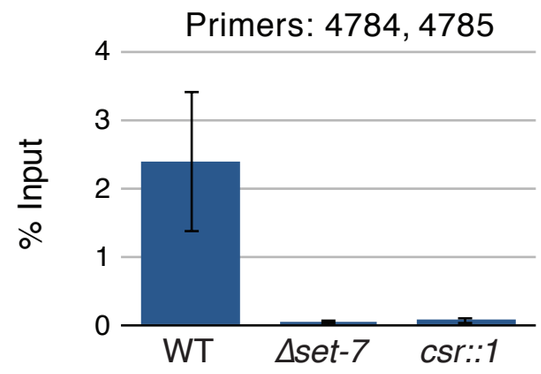

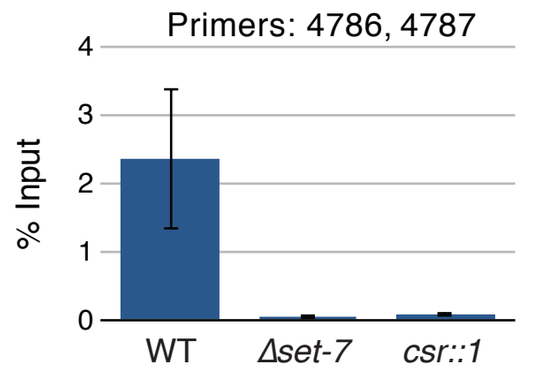

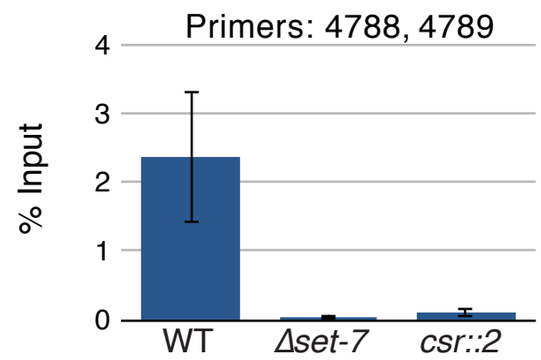

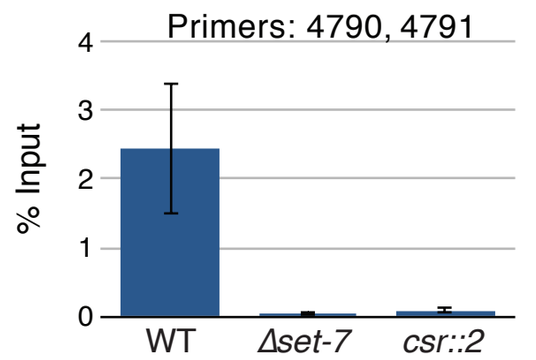

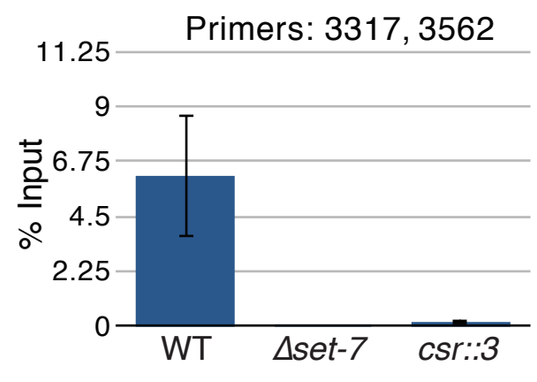

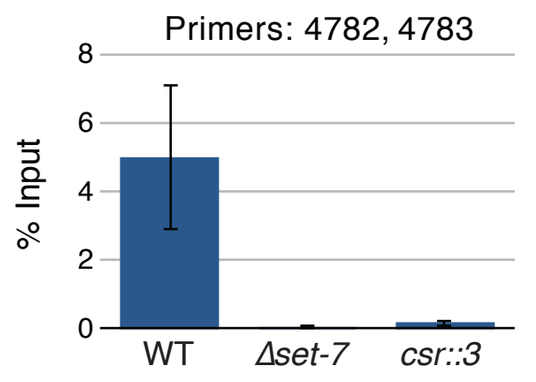

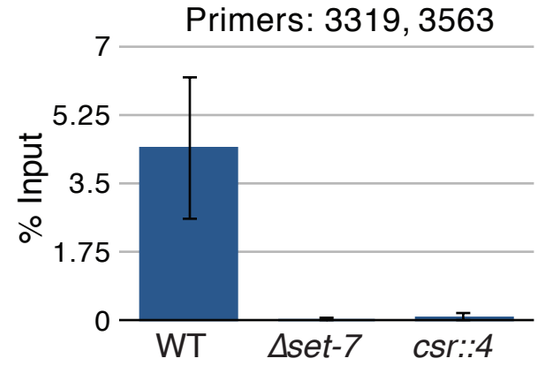

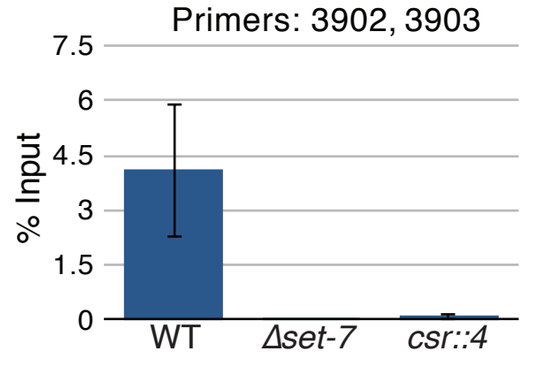

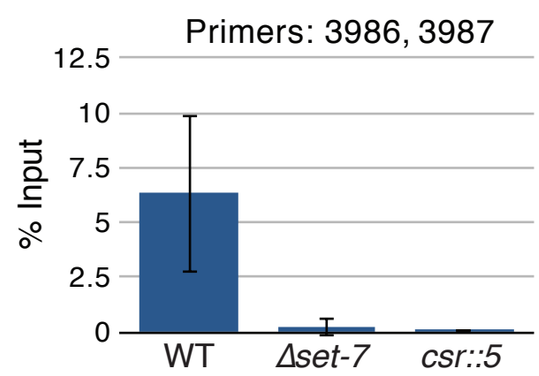

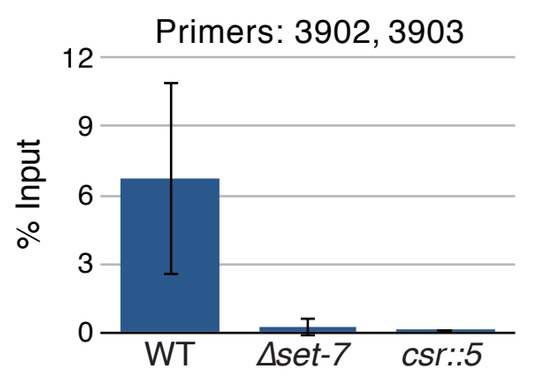

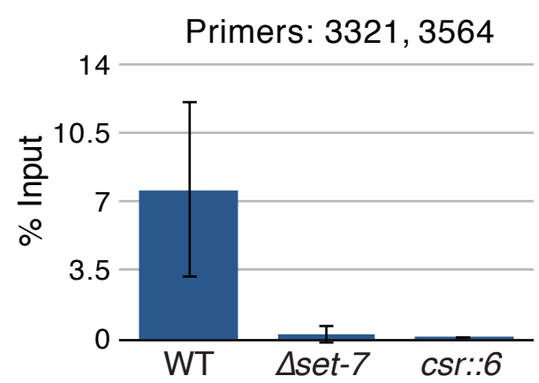

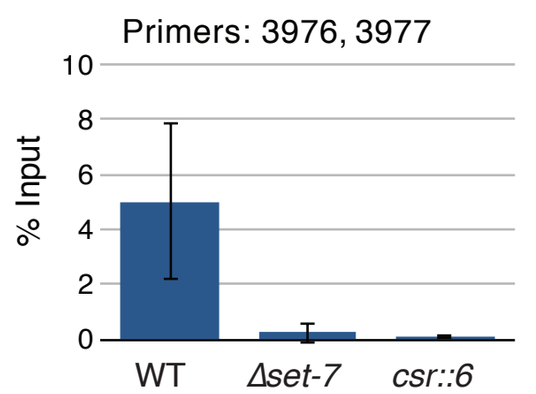

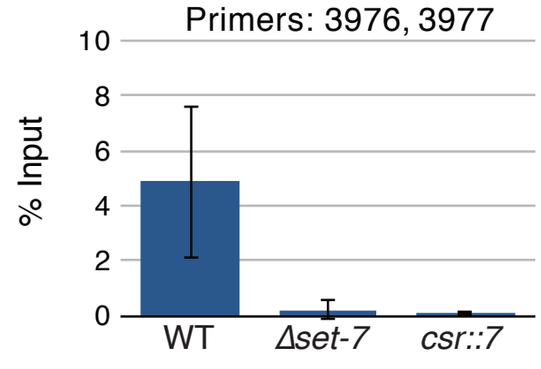

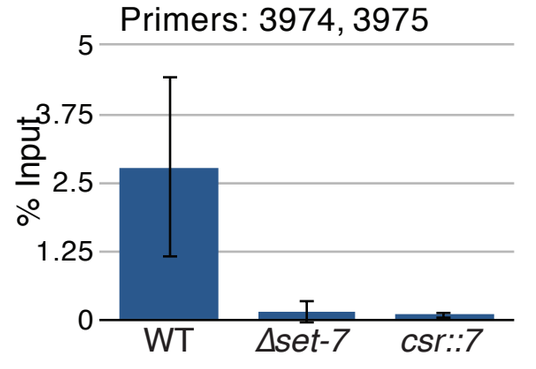

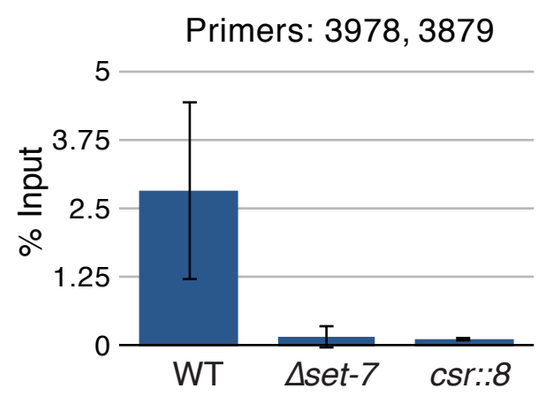

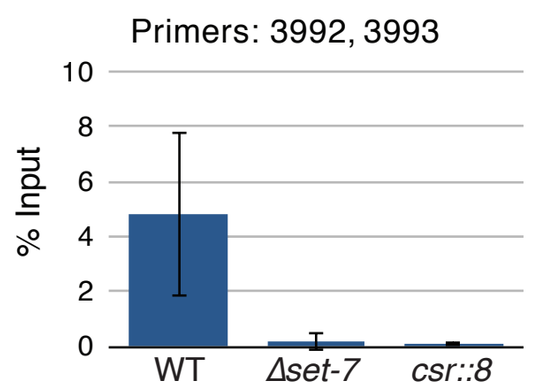

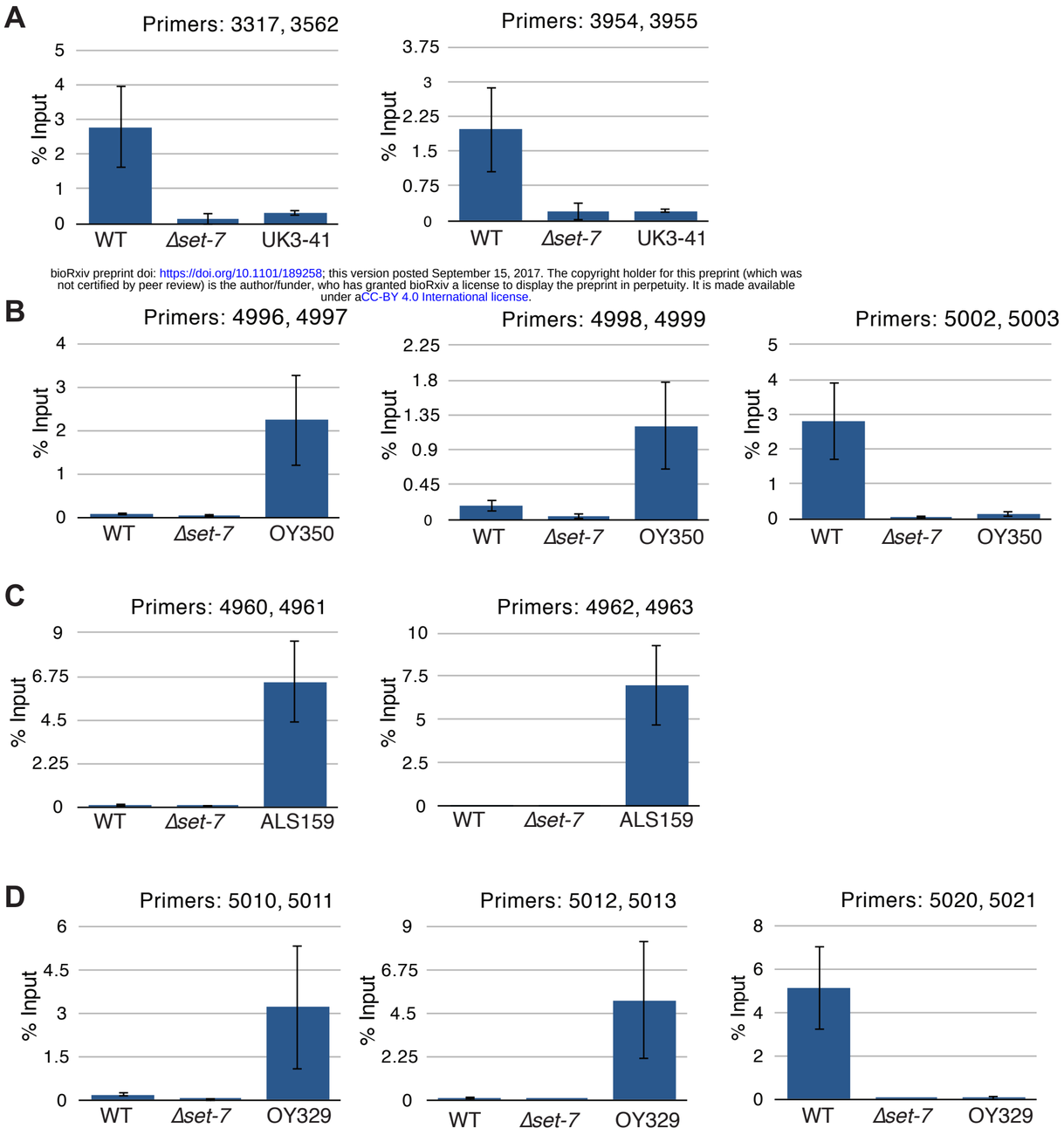

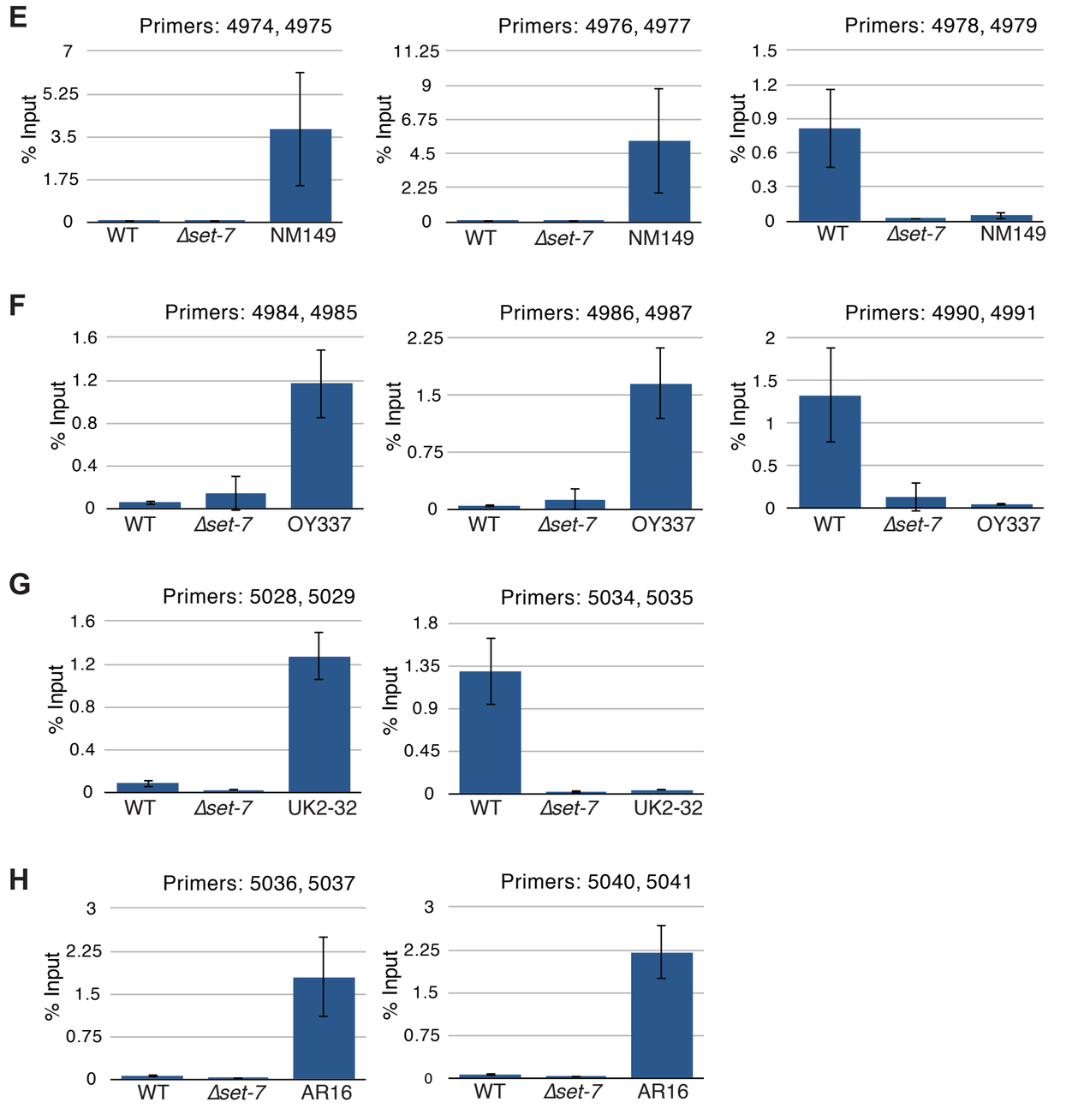

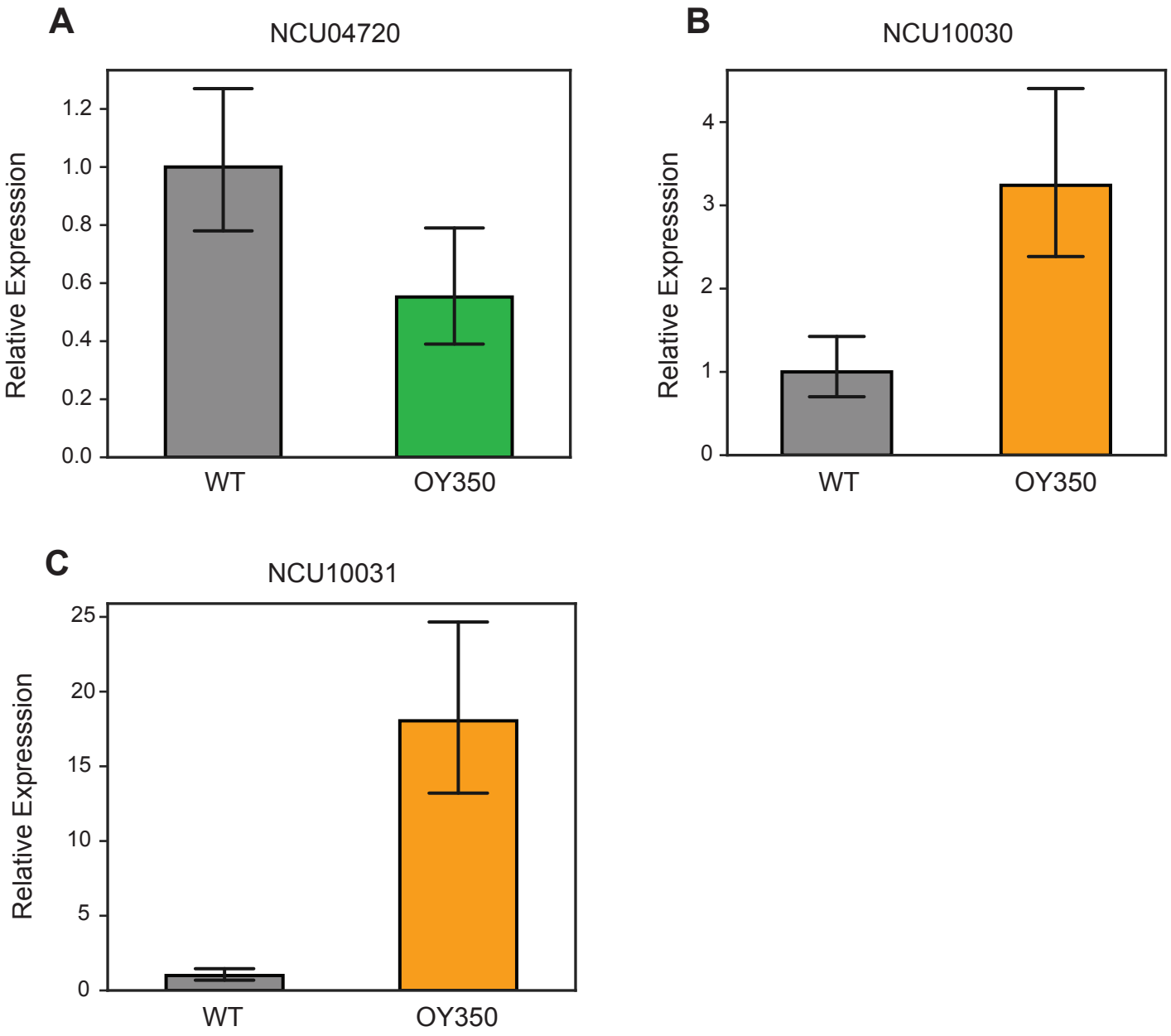

Jamieson_FigS4

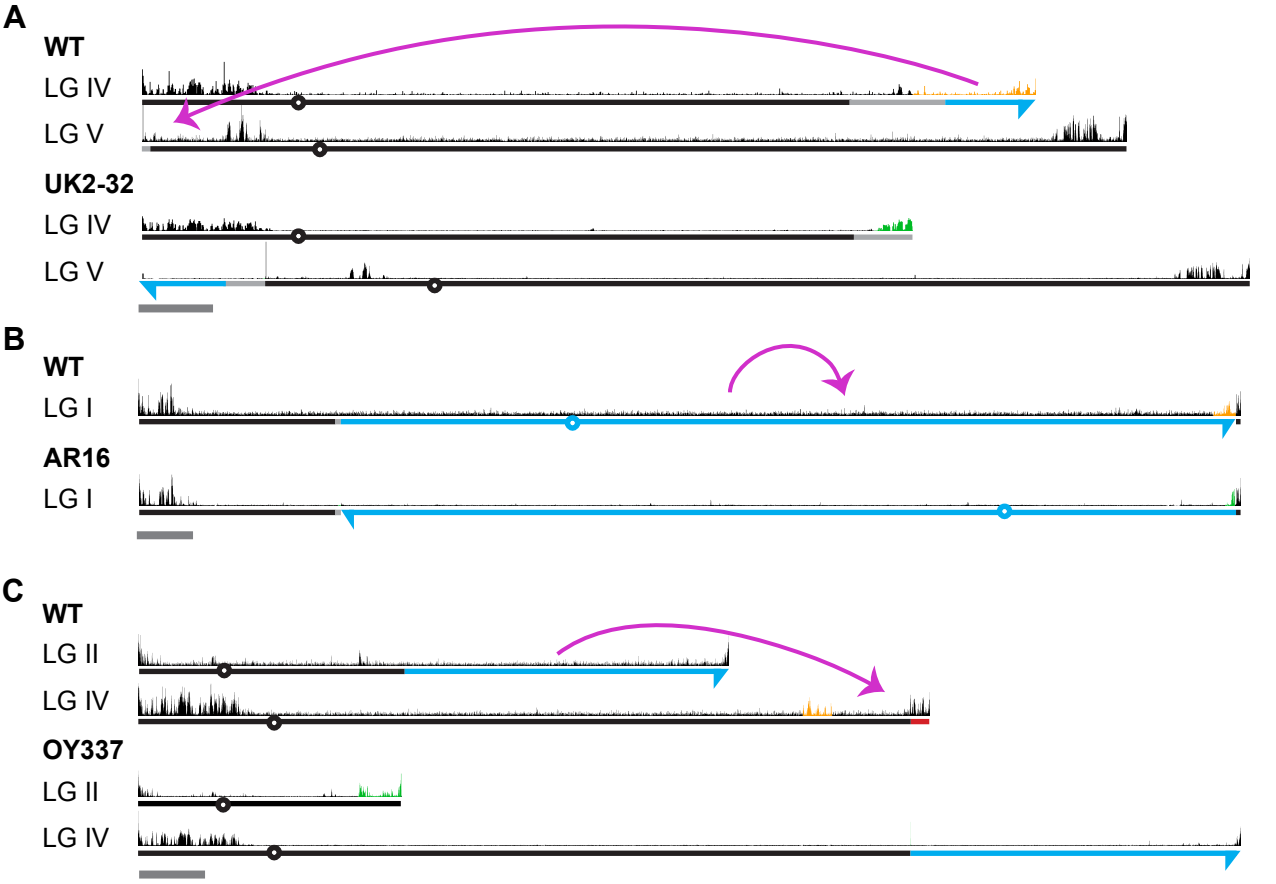

Jamieson_FigS5